University Library

MINERVA ACCESS

A gateway to Melbourne's research publications

Minerva Access is the Institutional Repository of The University of Melbourne

Author/s:
Snelson, M;Tan, SM;Clarke, RE;de Pasquale, C;Thallas-Bonke, V;Nguyen, T-V;Penfold, SA;Harcourt, BE;Sourris, KC;Lindblom, RS;Ziemann, M;Steer, D;El-Osta, A;Davies, MJ;Donnellan, L;Deo, P;Kellow, NJ;Cooper, ME;Woodruff, TM;Mackay, CR;Forbes, JM;Coughlan, MT

Title:
Processed foods drive intestinal barrier permeability and microvascular diseases.

Date:
2021-03

Citation:
Snelson, M., Tan, S. M., Clarke, R. E., de Pasquale, C., Thallas-Bonke, V., Nguyen, T. -V., Penfold, S. A., Harcourt, B. E., Sourris, K. C., Lindblom, R. S., Ziemann, M., Steer, D., El-Osta, A., Davies, M. J., Donnellan, L., Deo, P., Kellow, N. J., Cooper, M. E., Woodruff, T. M. ,... Coughlan, M. T. (2021). Processed foods drive intestinal barrier permeability and microvascular diseases.. Sci Adv, 7 (14), https://doi.org/10.1126/sciadv.abe4841.

Persistent Link:
https://hdl.handle.net/11343/277970

License:
CC BY-NC

HEALTH AND MEDICINE

Processed foods drive intestinal barrier permeability and microvascular diseases

Matthew Snelson[1]*, Sih Min Tan[1]*, Rachel E. Clarke[2], Cassandra de Pasquale[1], Vicki Thallas-Bonke[1], Tuong-Vi Nguyen[1], Sally A. Penfold[1], Brooke E. Harcourt[3], Karly C. Sourris[1], Runa S. Lindblom[1], Mark Ziemann[4], David Steer[5], Assam El-Osta[1], Michael J. Davies[6], Leigh Donnellan[7], Permal Deo[7], Nicole J. Kellow[8], Mark E. Cooper[1], Trent M. Woodruff[9], Charles R. Mackay[10,11], Josephine M. Forbes[12], Melinda T. Coughlan[1,13†]

Copyright © 2021 The Authors, some rights reserved; exclusive licensee American Association for the Advancement of Science. No claim to original U.S. Government Works. Distributed under a Creative Commons Attribution NonCommercial License 4.0 (CC BY-NC).

Intake of processed foods has increased markedly over the past decades, coinciding with increased microvascular diseases such as chronic kidney disease (CKD) and diabetes. Here, we show in rodent models that long-term consumption of a processed diet drives intestinal barrier permeability and an increased risk of CKD. Inhibition of the advanced glycation pathway, which generates Maillard reaction products within foods upon thermal processing, reversed kidney injury. Consequently, a processed diet leads to innate immune complement activation and local kidney inflammation and injury via the potent proinflammatory effector molecule complement 5a (C5a). In a mouse model of diabetes, a high resistant starch fiber diet maintained gut barrier integrity and decreased severity of kidney injury via suppression of complement. These results demonstrate mechanisms by which processed foods cause inflammation that leads to chronic disease.

INTRODUCTION

Processed foods are a key hallmark of the Western diet. There is now a growing body of evidence that processed foods are detrimental to human health (*1*). The availability and consumption of processed, thermally treated food has increased substantially over the past decades (*2*), in line with the obesity and diabetes pandemic (*3*, *4*). Obesity and diabetes associate with microvascular complications, particularly chronic kidney disease (CKD). CKD affects almost 14% of the general population (*5*) and is itself a major risk factor for cardiovascular disease and all-cause mortality (*6*).

One increasingly recognized and potentially pathogenic component of processed foods is a group of posttranslational modifications known as advanced glycation endproducts (AGEs). AGEs are generated from mixtures of amino acids and reducing sugars via the Maillard reaction (*7*) that takes place under heat conditions such as during thermal processing, which commonly occurs during food production and processing (*8*–*10*). Because the Maillard reaction induces chemical changes within foods that impart flavor and aroma (*11*), the food industry has long enhanced or supplemented Maillard reaction products in foods to increase sensory properties and palatability, and as such, AGEs are a ubiquitous component of processed (and particularly extensively heat-treated) foods. The consumption of processed foods containing these AGEs may underlie chronic disease risk (*8*).

Most of the diet-derived AGEs escape digestion and absorption and pass through the gastrointestinal tract to the colon (*12*, *13*). Here, they are available as substrates for gut microbial metabolism (*14*, *15*). However, the extent to which long-term intake of processed food impacts intestinal permeability and influences the outcome of microvascular disorders such as CKD is unclear. Consumption of processed foods has been linked to cancer (*16*), cardiovascular diseases (*17*, *18*), and all-cause mortality (*18*); thus, there is an urgent need to define the molecular mechanisms linking chronic intake of processed foods to the onset and progression of noncommunicable diseases.

RESULTS

A processed diet induces CKD associated with innate immune complement activation

To study the impact of processed diets on microvascular disease risk, we fed Sprague-Dawley rats a thermally processed diet for 24 weeks. Thermal processing is well documented to increase de novo AGE content within foodstuffs (*8*), and heat treatment of an unbaked rodent chow (AIN93G; table S1) for 60 min leads to an increase in the well-described AGEs N^{ϵ}-carboxymethyl lysine (CML), N^{ϵ}-carboxyethyl lysine (CEL), and fructosamine (table S2), without destroying heat-labile vitamins (table S2). Diets were supplied ad libitum and did not lead to increased food consumption or caloric intake (table S3). Chronic consumption of the heat-treated (HT) diet induced leakage of albumin into the urine, fivefold higher than that seen with unbaked control (Con) diet (Fig. 1A), consistent with kidney injury. Consumption of the heat-treated diet led to additional hallmarks of early CKD including renal hyperfiltration as indicated by increased creatinine clearance [a surrogate marker of glomerular

[1]Department of Diabetes, Central Clinical School, Alfred Medical Research and Education Precinct, Monash University, Melbourne, Victoria, Australia. [2]Monash Biomedicine Discovery Institute, Monash University, Clayton, Victoria, Australia. [3]Murdoch Children's Research Institute, Royal Children's Hospital, Melbourne, Victoria, Australia. [4]Deakin University, School of Life and Environmental Sciences, Geelong, Victoria, Australia. [5]Monash Proteomics and Metabolomics Facility, Monash University, Melbourne, Victoria, Australia. [6]Department of Biomedical Sciences, University of Copenhagen, Copenhagen, Denmark. [7]Health and Biomedical Innovation, School of Pharmacy and Medical Sciences, University of South Australia, Adelaide, South Australia, Australia. [8]Department of Nutrition, Dietetics and Food, Monash University, Melbourne, Victoria, Australia. [9]School of Biomedical Sciences, University of Queensland, Brisbane, Queensland, Australia. [10]Infection and Immunity Program, Monash Biomedicine Discovery Institute, Monash University, Melbourne, Victoria, Australia. [11]Department of Microbiology, Monash University, Melbourne, Victoria, Australia. [12]Glycation and Diabetes Group, Mater Research Institute—The University of Queensland, Translational Research Institute, Woolloongabba, Queensland, Australia. [13]Baker Heart and Diabetes Institute, Melbourne, Victoria, Australia.
*These authors contributed equally to this work.
†Corresponding author. Email: melinda.coughlan@monash.edu

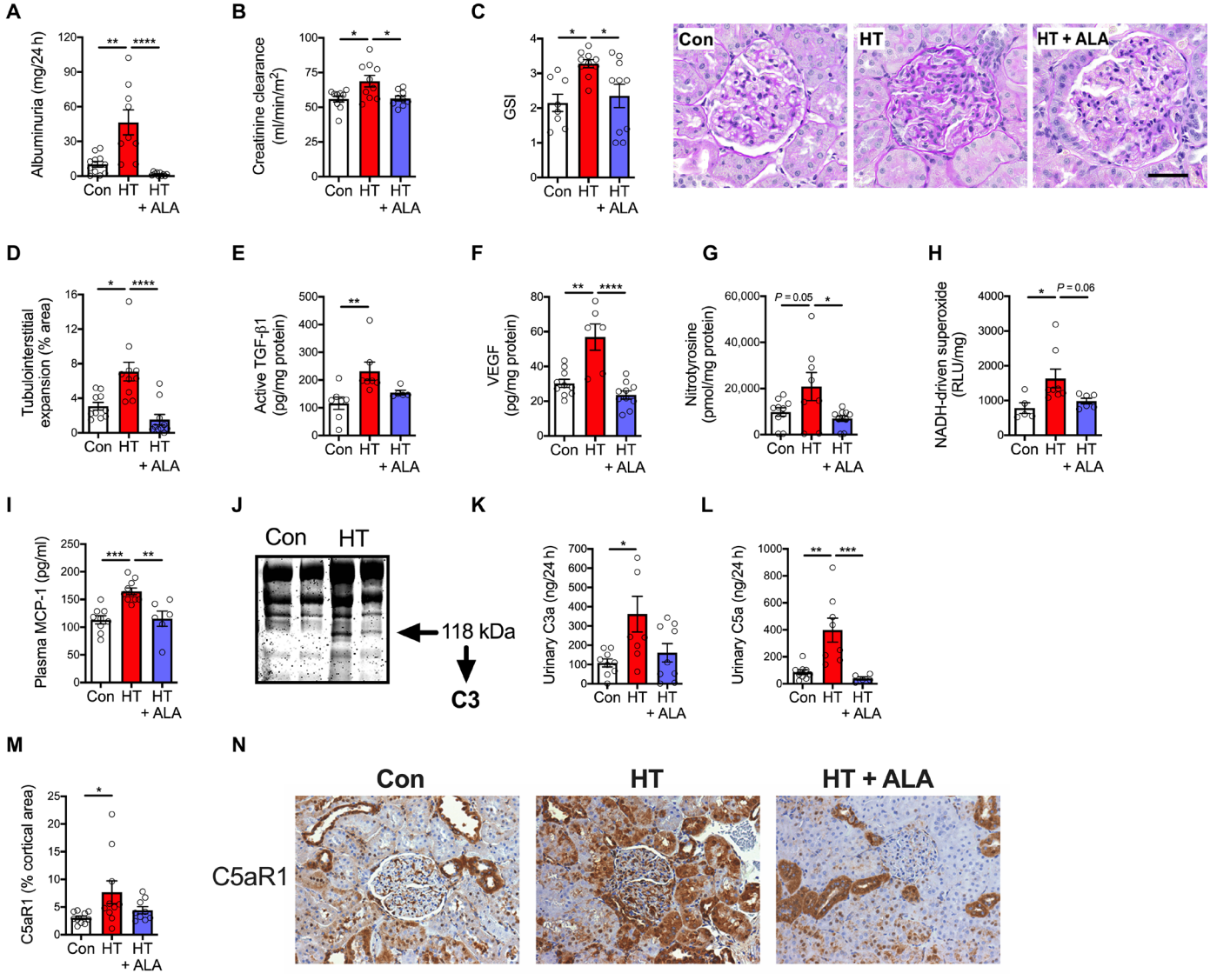

Fig. 1. Long-term consumption of a processed diet promotes low-grade systemic inflammation, complement activation, and CKD. Healthy rats were fed an untreated diet (Con; white), a processed heat-treated diet (HT; red), or a heat-treated diet plus the AGE inhibitor ALA (HT + ALA; blue) (10 mg/kg per day oral gavage for 24 weeks). (**A** and **B**) Kidney function. (A) Twenty-four–hour urinary excretion of albumin. (B) Creatinine clearance. (**C** and **D**) Kidney histology. (C) Glomerulosclerotic index (GSI) and representative PAS-stained kidney sections (right). Scale bar, 50 μm. (D) Renal tubulointerstitial expansion. (**E** and **F**) Prosclerotic cytokines measured in kidney cortex (E) active TGF-β1 protein and (F) VEGF. (**G** and **H**) Renal cortical oxidative stress markers (G) 3-nitrotyrosine and (H) mitochondrial superoxide generation. (**I**) Plasma levels of MCP-1. (**J**) SDS–polyacrylamide gel electrophoresis (SDS-PAGE) of rat serum shows the presence of a 118-kDa protein present in heat-treated diet–fed rats. MALDI-TOF MS identified this protein as complement component C3. (**K** and **L**) Urinary excretion of distal complement proteins (K) C3a and (L) C5a. (**M** and **N**) Immunostaining of kidney cortex for C5aR1 quantification (M) and localization (N). Data are means ± SEM. Dots represent individual rodents. *$P < 0.05$, **$P < 0.01$, ***$P < 0.001$, and ****$P < 0.0001$. *P* values were determined by one-way analysis of variance (ANOVA) with Tukey's multiple comparisons test; $n = 5$ to 10 rats per group.

filtration rate (GFR); Fig. 1B] and morphological changes to the glomeruli of the kidneys, a tuft of capillaries involved in blood filtration {glomerulosclerosis [glomerulosclerotic index (GSI)]; Fig. 1C}. Tubulointerstitial fibrosis is a prominent feature of progressive CKD. The heat-treated diet led to an increase in tubulointerstitial expansion (Fig. 1D), consistent with deposition of extracellular matrix components within the tubular interstitial space. Transforming growth factor–β1 (TGF-β1) is pivotal in driving renal fibrosis in CKD (*19*), and activation of TGF-β1 in the renal cortex was observed with chronic consumption of the heat-treated diet (Fig. 1E), in parallel with an increase in vascular endothelial growth factor (VEGF; Fig. 1F), an angiogenic cytokine, consistent with disruption to the microvascular architecture. Overproduction of reactive oxygen species (ROS) in the setting of CKD is thought to underlie the chronic inflammatory processes leading to renal fibrosis (*20*). Rats eating the heat-treated diet showed evidence of the oxidative stress response, localized to the kidney, with formation of 3-nitrotyrosine adducts (Fig. 1G) and mitochondrial superoxide generation (Fig. 1H), a key site of ROS generation. The inflammatory chemokine monocyte chemoattractant protein–1 (MCP-1) was increased with

high-AGE feeding (Fig. 1I), suggesting that processed food can incite a "sterile" inflammatory response.

To explore whether the AGE component of the processed diet was responsible for the kidney phenotype observed with chronic feeding of the heat-treated diet, we administered an inhibitor of the AGE pathway, alagebrium chloride (ALA). Consistent with the hypothesis that the pathogenic effects of heat-treated diets are due to AGEs, we observed that pharmacological treatment of heat-treated–fed rats with ALA (10 mg/kg per day) by oral gavage mitigated renal injury (Fig. 1, A to D and F), renal fibrosis (Fig. 1E), the oxidative stress response (Fig. 1, G and H), and systemic inflammation (Fig. 1I).

To gain insight into heat-treated diet–induced systemic factors that might be causative in renal disease progression, rat serum was separated by polyacrylamide gel electrophoresis. Visualization of protein bands revealed the presence of bands at approximately 118 kDa, uniquely observed in serum from the heat-treated diet animals (Fig. 1J). Excision of the bands and subsequent peptide mass fingerprinting using matrix-assisted laser desorption/ionization–time-of-flight (MALDI-TOF) mass spectrometry (MS)–based proteomics identified these unique protein bands as complement component C3. The innate immune complement system is a highly sophisticated network of proteins that are activated in response to invading pathogens or tissue injury. This system is finely balanced and, when subject to states of dysregulation or hyperactivation, can propagate a potent inflammatory response. Complement comprises four mechanistic pathways: classical, lectin, alternative, and extrinsic. Activation of any one of these converges to the production of the complement C3 and C5 convertases, which cleave complement C3 and C5, respectively, resulting in the generation of the opsonic C3b and anaphylatoxins C3a and C5a and subsequently the formation of membrane attack complex (MAC; comprising C5b-9) (*21*). All complement activation pathways result in the formation of C5a, a potent and major effector molecule of the complement system, which, via ligation with the receptor C5aR1, initiates and propagates pathology in inflammatory disease states (*22*). Accordingly, to verify the effects of the heat-treated diet on complement activation, we measured concentrations of the complement effector molecules distal to the cascade, C3a (Fig. 1K) and C5a (Fig. 1L), which were both increased in the urine of rats receiving the heat-treated diet, and notably, C5a was attenuated with the AGE-lowering therapy (ALA), suggesting regulation through the AGE pathway. Immunostaining of the kidney cortex for the C5a receptor C5aR1 demonstrated localization predominantly to the renal tubules and to the glomeruli, with the abundance of this receptor increased with the heat-treated diet (Fig. 1, M and N). Together, these data demonstrate that chronic consumption of processed diets can lead to kidney injury, profibrotic changes, and complement pathway activation as a direct result of the AGE content of the diet.

Complement anaphylatoxin signaling is obligatory for processed diet–induced microvascular injury

To determine whether C5a signaling is necessary for the development of kidney injury as a result of consumption of a processed diet, the in vivo heat-treated diet model was repeated for 24 weeks with the addition of a group of rats dosed daily with an orally active C5aR1 inhibitor, PMX53 (*23*), 2 mg/kg per day by oral gavage. Inhibition of C5a signaling via PMX53 administration prevented heat-treated diet–induced albuminuria (Fig. 2A), renal hyperfiltration (Fig. 2B), and reduced GSI (Fig. 2, C and D). Active TGF-β1 (Fig. 2D), mitochondrial superoxide production (Fig. 2F), and MCP-1 (Fig. 2G) were each dampened with pharmacological C5aR1 inhibition.

C3a, generated via cleavage of C3, is the other anaphylatoxin produced by the complement cascade. To ascertain whether C3a activation is required for kidney injury resulting from chronic consumption of a heat-treated diet, we fed mice deficient in the C3a receptor ($C3aR^{-/-}$ mice) a heat-treated diet for 24 weeks. Genetic deletion of C3aR mitigated heat-treated diet–induced changes in kidney function [creatinine clearance (Fig. 3A)], but not albuminuria (Fig. 3B), structural injury (GSI; Fig. 3, C and D), or fibrosis (active TGF-β1; Fig. 3E). Urinary markers of tubular injury (Kim-1; Fig. 3F) and oxidative stress (15-isoprostane F_{2t}; Fig. 3G) were induced by the heat-treated diet, and this increase was ameliorated with deletion of the C3a receptor.

These data provide further evidence that chronic consumption of a processed diet induces kidney injury and that blockade of the proinflammatory effector molecule C5a prevents these changes, indicating the crucial role of the complement pathway in the development of heat-treated diet–induced kidney dysfunction.

Processed diets promote intestinal barrier permeability and redistribution of the gut commensal consortium

Increased intestinal permeability leads to inflammation and chronic disease risk (*24*). When intestinal epithelial tight junction proteins are compromised, microbial molecules such as lipopolysaccharide (LPS) translocate from the gut into the systemic circulation. Bacterial products trigger the innate immune system, resulting in chronic inflammation. To explore whether processed diets can drive intestinal permeability, LPS levels were determined in the serum of rats consuming the heat-treated diet. Rats eating the heat-treated diet for 24 weeks had increased serum LPS, which was reversed with either the AGE inhibitor alagebrium (Fig. 4A) or the C5aR1 inhibitor (Fig. 4B), suggesting that changes in gut permeability are involved in the effects of processed food and mediated by complement signaling.

Diet is a key determinant of gut microbiota diversity and abundance (*25*). To examine the effects of processed diet consumption on the gut microbiota profile, C57BL/6 mice were fed a heat-treated diet for 24 weeks and cecal digesta underwent 16*S* ribosomal RNA (rRNA) sequencing. Principal coordinates analysis (PCoA) based on unweighted UniFrac demonstrated that the diets clustered independently (Fig. 4C). Alpha diversity of cecal microbiota, as measured by Simpson's diversity index, was not altered in mice fed the heat-treated diet (Fig. 4D). Using linear discriminant analysis (LDA) coupled with effect size measurements [LEfSe (*26*)], we next determined which taxa were enriched in mice receiving a heat-treated diet (Fig. 4, E and F). Notably, Epsilonproteobacteria were enriched with the heat-treated diet (Fig. 4, E and F), driven by an expansion in *Helicobacteraceae* (Fig. 4G). The most contracted feature, as measured by LDA score, was Saccharibacteria (previously known as TM7) (Fig. 4H). Consistent with our studies in rats (Fig. 1), the heat-treated diet led to a CKD phenotype shown by albuminuria (Fig. 4I), a change in renal function (hyperfiltration, as shown by plasma cystatin C; Fig. 4J), increased circulating MCP-1 (Fig. 4K), and LPS (Fig. 4L). Gene expression of the tight junction proteins occludin and claudin-1 was down-regulated in the jejunum (Fig. 4, M and N), and claudin-5 was up-regulated in the jejunum (Fig. 4O), raising the possibility that the intestinal epithelial barrier might be

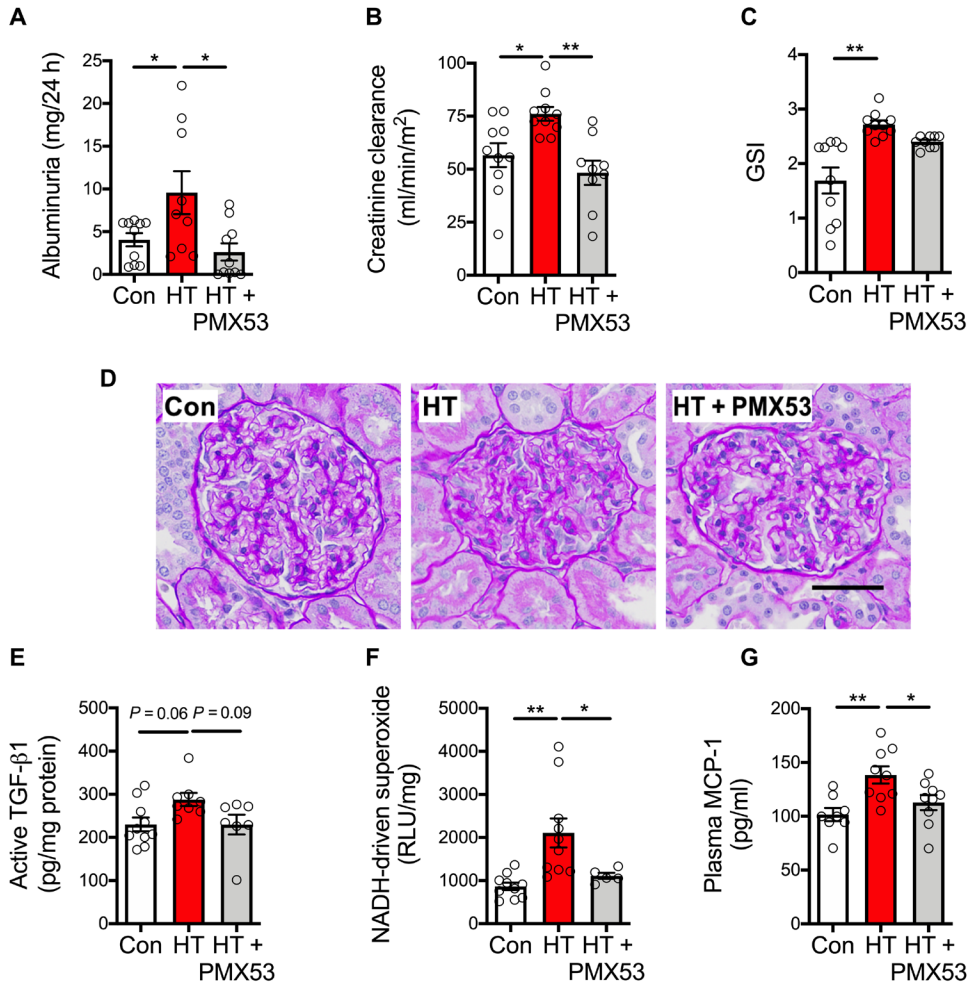

Fig. 2. Pharmacological inhibition of the C5aR1 receptor ameliorates kidney damage, low-grade inflammation, and ROS generation resulting from chronic consumption of a processed diet. Healthy rats were fed either a control (Con; white) or heat-treated (HT; red) diet for 24 weeks with or without administration of the C5aR1 antagonist PMX53 (2 mg/kg per day oral gavage; gray). (**A**) Twenty-four–hour urinary excretion of albumin. (**B**) Creatinine clearance. (**C**) GSI and (**D**) representative PAS-stained kidney sections. Scale bar, 50 μm. (**E**) Active TGF-β1 protein in kidney. (**F**) Kidney mitochondrial superoxide. (**G**) Plasma MCP-1. Data are means ± SEM. Dots represent individual rodents. *$P < 0.05$ and **$P < 0.01$. *P* values were determined by one-way ANOVA with Tukey's multiple comparisons test; $n = 5$ to 10 rats per group.

altered by the processed food diet. However, at this site, zonula occludens-1 (*Tjp-1*) was unchanged (Fig. 4P). In the ileum, while the heat-treated diet did not affect the gene expression of occludin (Fig. 4Q) or zonula occludens-1 (Fig. 4T), claudin-1 and claudin-5 were markedly up-regulated (Fig. 4, R and S). The same pattern of tight junction protein expression was seen in the colon (fig. S4, A to D). Together, these results suggest that intestinal epithelial integrity may be compromised by overconsumption of a processed food diet.

To ascertain whether complement is up-regulated at the level of the intestine as a result of eating a heat-treated diet, intestinal expression of complement C3 and C5 was determined. C3 was unchanged in ileum (fig. S5A) and jejenum (fig. S5B) of mice eating a heat-treated diet, and C5 expression was undetectable (fig. S5), supporting the hypothesis that complement is activated distal to the gut (i.e., within the circulation). This was verified by in vitro studies using Caco-2 cells exposed to AGEs. Incubation of Caco-2 cells with AGEs for 24 hours led to an increase in the expression of the tight junction protein JAMA (fig. S6A), but no change in cellular complement (C3, C5, and C5aR1) was observed (fig. S6, B to D). There was no change in C5a release into the incubation medium after AGE exposure (fig. S6E).

Consumption of a processed diet increases risk of microvascular disease via intestinal barrier permeability

To further explore the effects of processed diets on the intestinal epithelial barrier and microvascular disease risk, a model susceptible to the development of CKD, the spontaneously diabetic leptin receptor–deficient ($Lepr^{db/db}$) mouse was studied. Exposure of $Lepr^{db/db}$ mice to the heat-treated "processed" diet for 10 weeks led to enhanced albuminuria compared to $Lepr^{db/db}$ mice consuming an unbaked rodent chow (Fig. 5A). GFR, as shown by the surrogate measure creatinine clearance, was elevated in nondiabetic *db/m* mice eating the heat-treated diet, indicating hyperfiltration, and declined in $Lepr^{db/db}$ mice fed the heat-treated diet, which typically occurs as kidney disease progresses to a more advanced stage (Fig. 5B). In $Lepr^{db/db}$ mice, intestinal tight junction integrity was

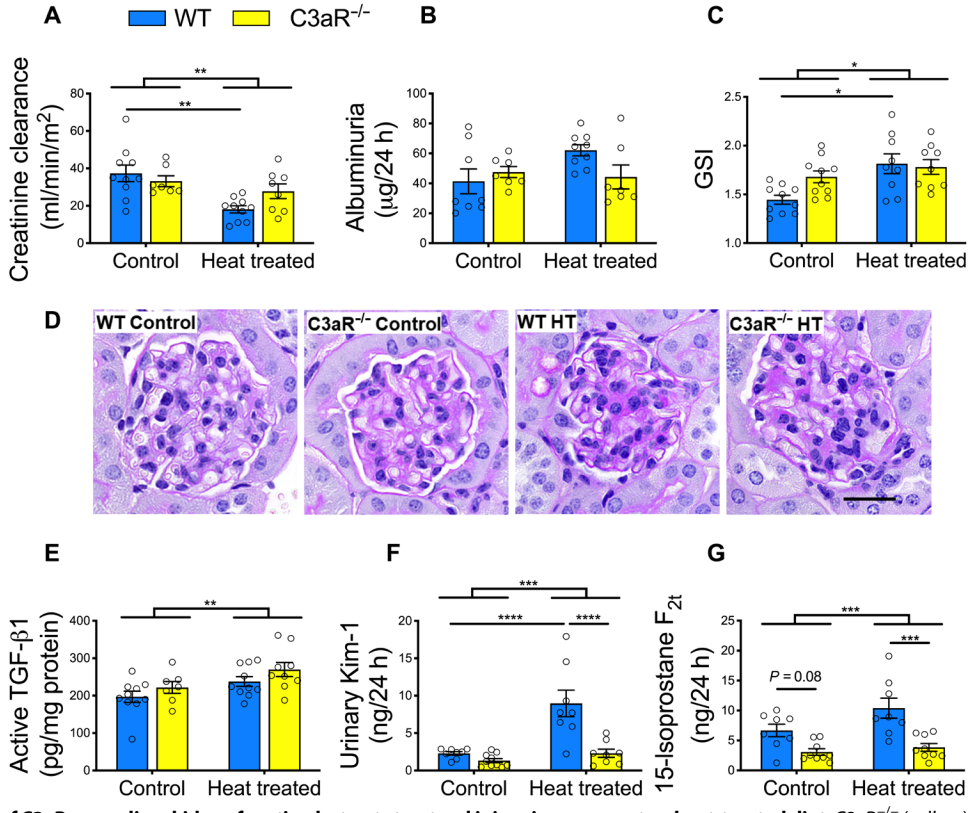

Fig. 3. Genetic deletion of C3aR normalizes kidney function but not structural injury in response to a heat-treated diet. C3aR$^{-/-}$ (yellow) and wild-type (blue) mice were fed an unbaked (Control) or heat-treated diet for 24 weeks. (**A**) Creatinine clearance. (**B**) Twenty-four–hour urinary excretion of albumin. (**C**) GSI and (**D**) representative PAS-stained kidney sections. Scale bar, 50 μm. (**E**) Kidney active TGF-β1 protein. (**F**) Urinary kidney injury molecule-1 (Kim-1) excretion. (**G**) Urinary 15-isoprostane F_{2t}. Data are means ± SEM. Dots represent individual rodents. *P < 0.05, **P < 0.01, ***P < 0.001, and ****P < 0.0001. P values were determined by two-way ANOVA with Tukey's multiple comparisons test; n = 7 to 10 mice per group.

compromised with enhanced influx of luminal molecules across the epithelial barrier (Fig. 5C). Ten weeks of feeding a processed diet further deteriorated gut barrier function in the setting of diabetes (Fig. 5C). These results provide convincing evidence that processed diets can drive intestinal barrier dysfunction and microvascular disease risk.

A high-fiber, resistant starch diet prevents impaired gut barrier function and improves severity of renal injury via suppression of complement

Dietary fiber has long been linked to beneficial effects in gastrointestinal inflammatory disorders and protection from colon cancer (*27*); however, there is a growing body of evidence that dietary fiber has consequences on inflammation outside of the intestine and may have health-promoting properties in organs distal to the gut (*28*, *29*). Resistant starch is a prebiotic fiber that is resistant to digestion in the small intestine and passes to the large intestine, where it is fermented by colonic bacteria. Accordingly, we used resistant starch supplementation, in the form of high-amylose maize starch type 2 (HAMS-R2), to target the gut microbiome in the *Lepr*$^{db/db}$ mouse model. The resistant starch supplemented diet reversed albuminuria in heat-treated diet–fed *Lepr*$^{db/db}$ mice (Fig. 5A, orange bars), but did not affect creatinine clearance (Fig. 5B). Fibronectin, a key marker of fibrosis, was increased in the kidney of *Lepr*$^{db/db}$ mice and was further up-regulated with consumption of the heat-treated diet and normalized with resistant starch (Fig. 5D).

Next, we sought to evaluate glucose handling in response to consumption of the prebiotic. We found that *Lepr*$^{db/db}$ mice consuming the resistant starch supplement had no change in fasting blood glucose (fig. S1A) or plasma insulin (fig. S1B), which translated to no change in Homeostatic Model Assessment of Insulin Resistance (HOMA-IR) (fig. S1C). In response to an oral glucose challenge [oral glucose tolerance test (OGTT)], there was no change in blood glucose (fig. S1D) or plasma insulin (fig. S1E), with resistant starch seen within the diabetic group (*Lepr*$^{db/db}$). Similarly, within mice with diabetes (*Lepr*$^{db/db}$), there were no changes in long-term glucose control (GHb; fig. S1F), fat mass (fig. S1G), or lean mass (fig. S1H) with resistant starch consumption. We next determined whole-body oxygen consumption (fig. S1I), respiratory rate (fig. S1J), and physical activity (fig. S1K) and found that, while there was a decrease in the setting of diabetes, resistant starch did not affect these parameters. These data indicate that the renoprotective effect of resistant starch supplementation occurred independent of changes in body composition or glycemic control.

Our earlier studies in the *Lepr*$^{db/db}$ mouse (Fig. 5) revealed that the processed diet led to an increase in intestinal permeability. When *Lepr*$^{db/db}$ mice consuming the heat-treated diet were supplemented with resistant starch, intestinal tight junction integrity was not altered compared to the control diet as shown by dextran–fluorescein isothiocyanate (FITC) appearance in the plasma (Fig. 5C). To determine whether the processed diet affected the cecal microbiome in *Lepr*$^{db/db}$ mice, 16*S* rRNA sequencing of DNA extracted

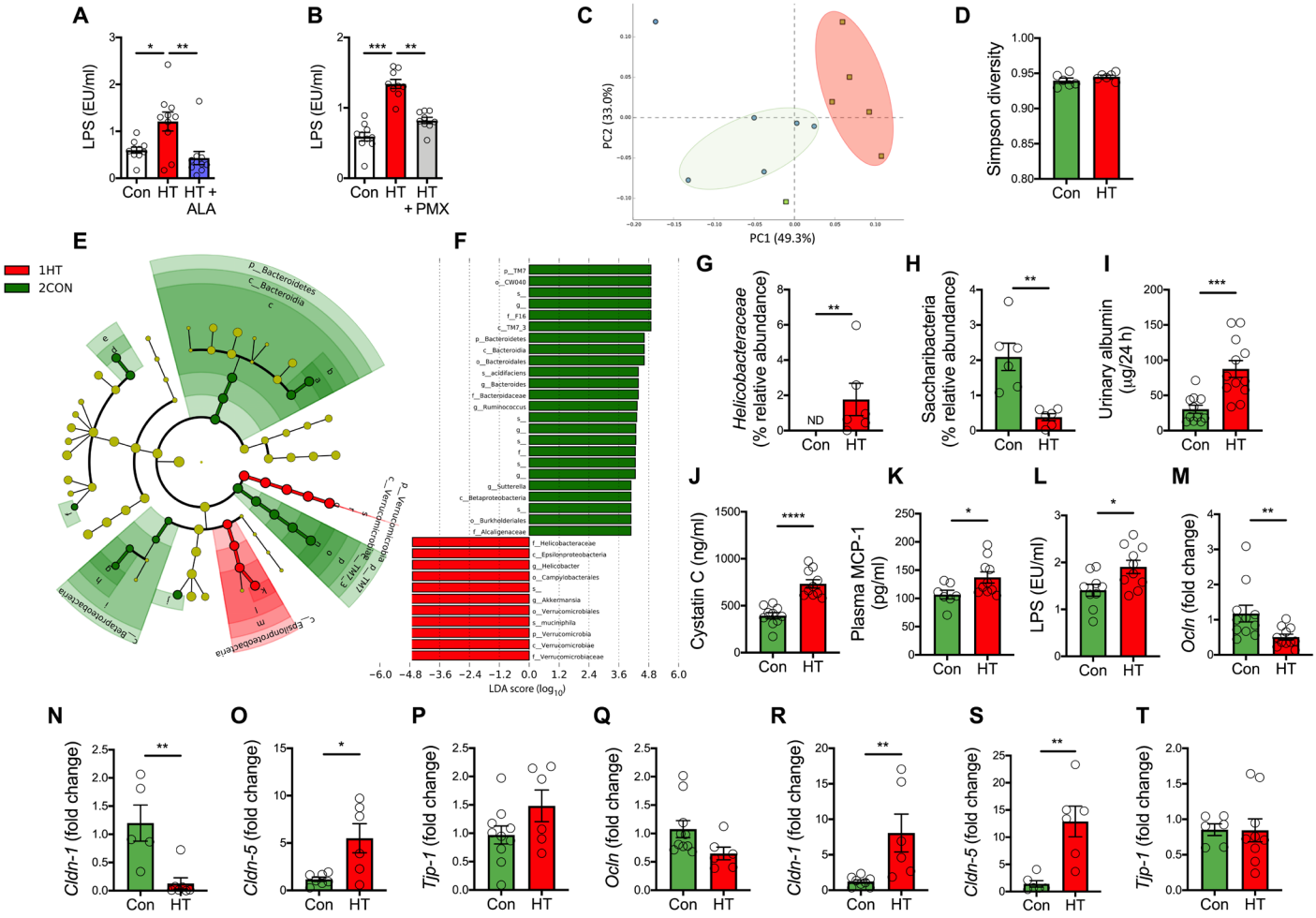

Fig. 4. Processed diets promote intestinal barrier permeability and redistribution of the gut commensal consortium. (**A**) Serum LPS in rats receiving an untreated diet (Con, white), a processed heat-treated diet (HT; red), or a heat-treated diet plus the AGE inhibitor ALA (HT + ALA; blue) (10 mg/kg per day oral gavage for 24 weeks). (**B**) Serum LPS in rats receiving either a heat-treated (red) diet for 24 weeks plus or minus the C5aR1 antagonist PMX53 (2 mg/kg per day oral gavage, gray). (**C** to **M**) C57BL/6 mice were fed either control (Con; green) or heat-treated (red) diets for 24 weeks, and cecal digesta underwent 16*S* rRNA sequencing: (C) PCoA (unweighted UniFrac) of cecal digesta. Green (bottom left), control unbaked diet; red (top right), heat-treated processed diet. (D) Simpson's diversity. (E) Cladogram and (F) LDA score plot illustrating the differences in the microbiota seen in C57BL/6 mice between those fed a heat-treated diet and control diet. (G) Relative abundance of *Helicobacteraceae*. (H) Relative abundance of Saccharibacteria. Heat-treated diet–fed C57BL/6 mouse: (I) 24-hour urinary excretion of albumin. (J) Plasma cystatin C. (K) Plasma MCP-1. (L) Plasma LPS. Jejunum expression of (M) occludin, (**N**) claudin-1, (**O**) claudin-5, and (**P**) zonula occludens-1 (*Tjp-1*). Ileum expression of (**Q**) occludin, (**R**) claudin-1, (**S**) claudin-5, and (**T**) zonula occludens-1 (*Tjp-1*). Data are displayed as means ± SEM. Dots represent individual rodents. *$P < 0.05$, **$P < 0.01$, ***$P < 0.001$, and ****$P < 0.0001$. *P* values were determined by one-way ANOVA with Tukey's multiple comparisons test (A and B), $n = 10$ rats per group; two-tailed unpaired Mann-Whitney *U* test (D and G to M), $n = 4$ to 6 mice per group for microbiome analysis; $n = 7$ to 12 mice per group for other analyses.

from cecal digesta was performed and data showed that consumption of the heat-treated diet in the setting of diabetes led to an increase in the Firmicutes to Bacteroidetes ratio (Fig. 5E). Resistant starch supplementation is known to increase the presence of beneficial saccharolytic butyrate-producing bacterial species in the colon. The resistant starch diet promoted changes in gut microbial ecology, reversing the heat-treated diet–induced increase in the Firmicutes/Bacteroidetes ratio (Fig. 5E), driven mainly by alterations in Bacteroidia class (Fig. 5F). In diabetic mice, the heat-treated diet was associated with a fourfold increase in the abundance of *Enterobacteriaceae*, previously observed to be elevated in patients with CKD (*30*), which was reduced with resistant starch supplementation (Fig. 5G). Next, we used LDA coupled with effect size measurements [LEfSe (*26*)] to determine which taxa were enriched in diabetic mice receiving a heat-treated diet. Consistent with our previous experiment in C57BL/6 mice, we observed that a heat-treated diet was associated with enrichment of Verrucomicrobia, while Bacteroidetes was reduced (Fig. 5, H and I).

There is intense interest in delineating the interactions between nutrition, gut microbiota, and gene regulation pathways in organs distal to the gut, such as the kidney. To provide mechanistic insight into processed food-induced kidney injury in the setting of diabetes, we performed transcriptomics of the kidneys from diabetic mice that had received the control diet, a heat-treated diet, and heat-treated diet supplemented with resistant starch ($n = 5$ per group). A heatmap showing hierarchical clustering of gene pathways is shown in Fig. 6A. Resistant starch supplementation reversed the gene changes observed with heat-treated diets in $Lepr^{db/db}$ mice, as shown in

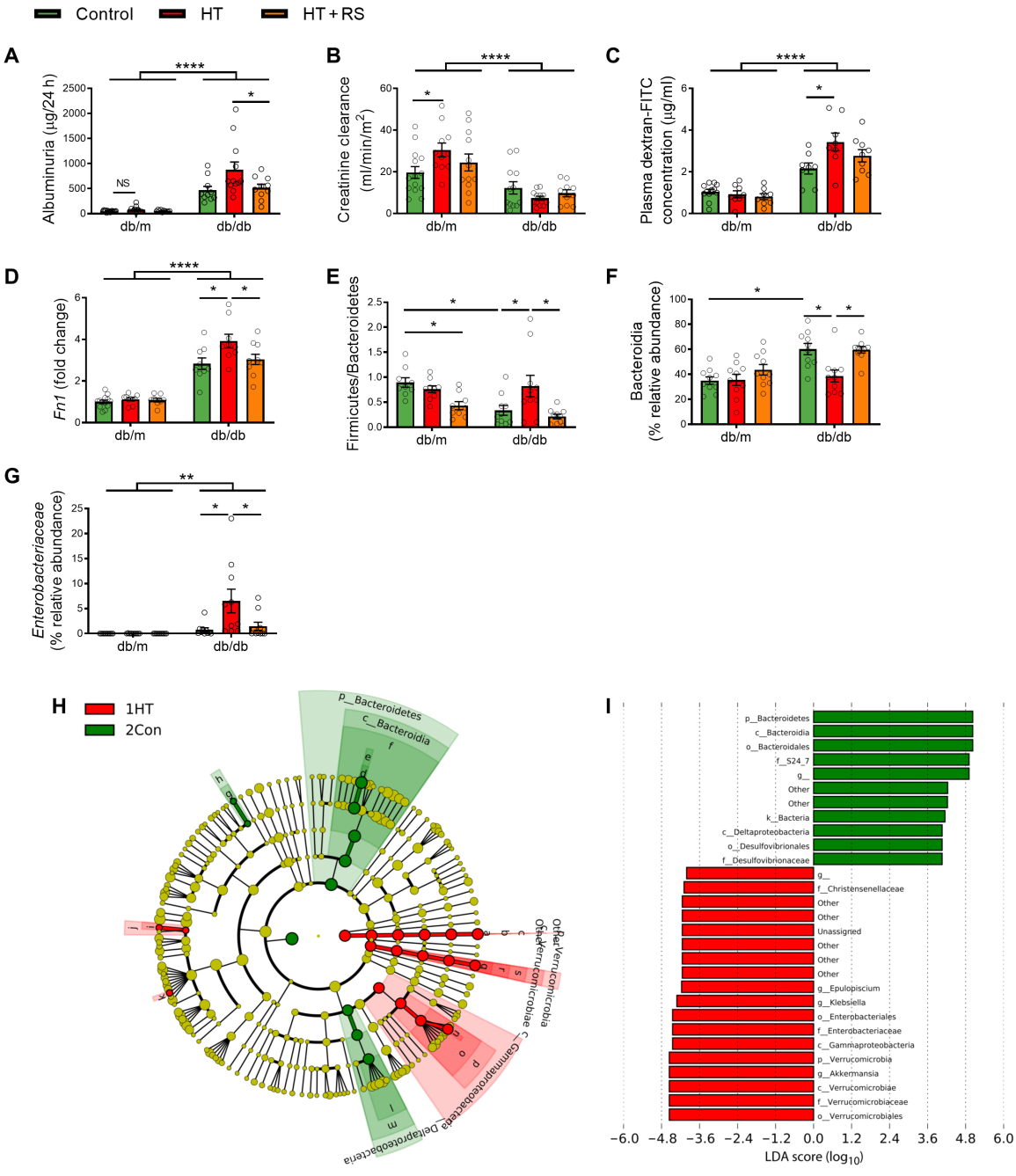

Fig. 5. Consumption of a processed diet increases risk of diabetic kidney disease, which can be improved by resistant starch fiber. Spontaneously diabetic leptin receptor–deficient (*Lepr*$^{db/db}$) and *db/m* (nondiabetic control) mice were fed an unbaked control diet (green), a heat-treated diet (red), or a heat-treated diet supplemented with resistant starch (high-amylose maize starch) (HT + RS; orange) for 10 weeks, and kidney function, intestinal permeability, and gut microbial ecology were determined. (**A**) Twenty-four–hour urinary excretion of albumin. (**B**) Creatinine clearance. (**C**) In vivo intestinal permeability. (**D**) Kidney fibronectin expression. (**E** to **I**) Cecal digesta underwent 16*S* rRNA sequencing: (E) Firmicutes/Bacteroidetes ratio. (F) Relative abundance of Bacteroidia. (G) Relative abundance of *Enterobacteriaceae*. (H) Cladogram and (I) LDA score plot illustrating the differences in the microbiota seen in diabetic mice between those fed a heat-treated diet and those receiving a control diet. Data are means ± SEM. Dots represent individual rodents. **P* < 0.05, ***P* < 0.01, ****P* < 0.001, and *****P* < 0.0001. *P* values were determined by two-way ANOVA with Tukey's multiple comparisons test, *n* = 8 to 16 mice per group.

Fig. 6B. Reactome gene set enrichment analysis (GSEA) showed up-regulation of immune signaling pathways due to the heat-treated diet and subsequent down-regulation with resistant starch supplementation (Fig. 6C), most notably signaling via cytokines and class A1 rhodopsin-like receptors and GPCR (G protein–coupled receptor) ligand binding. Further analysis using the more comprehensive MSigDB database showed tumor necrosis factor–α (TNF-α) signaling via nuclear factor κB (NF-κB) to be up-regulated in *Lepr*$^{db/db}$ mice fed a heat-treated diet [compared with mice fed a control diet, normalized enrichment score (NES) = 5.97, false discovery rate (FDR) < 0.001;

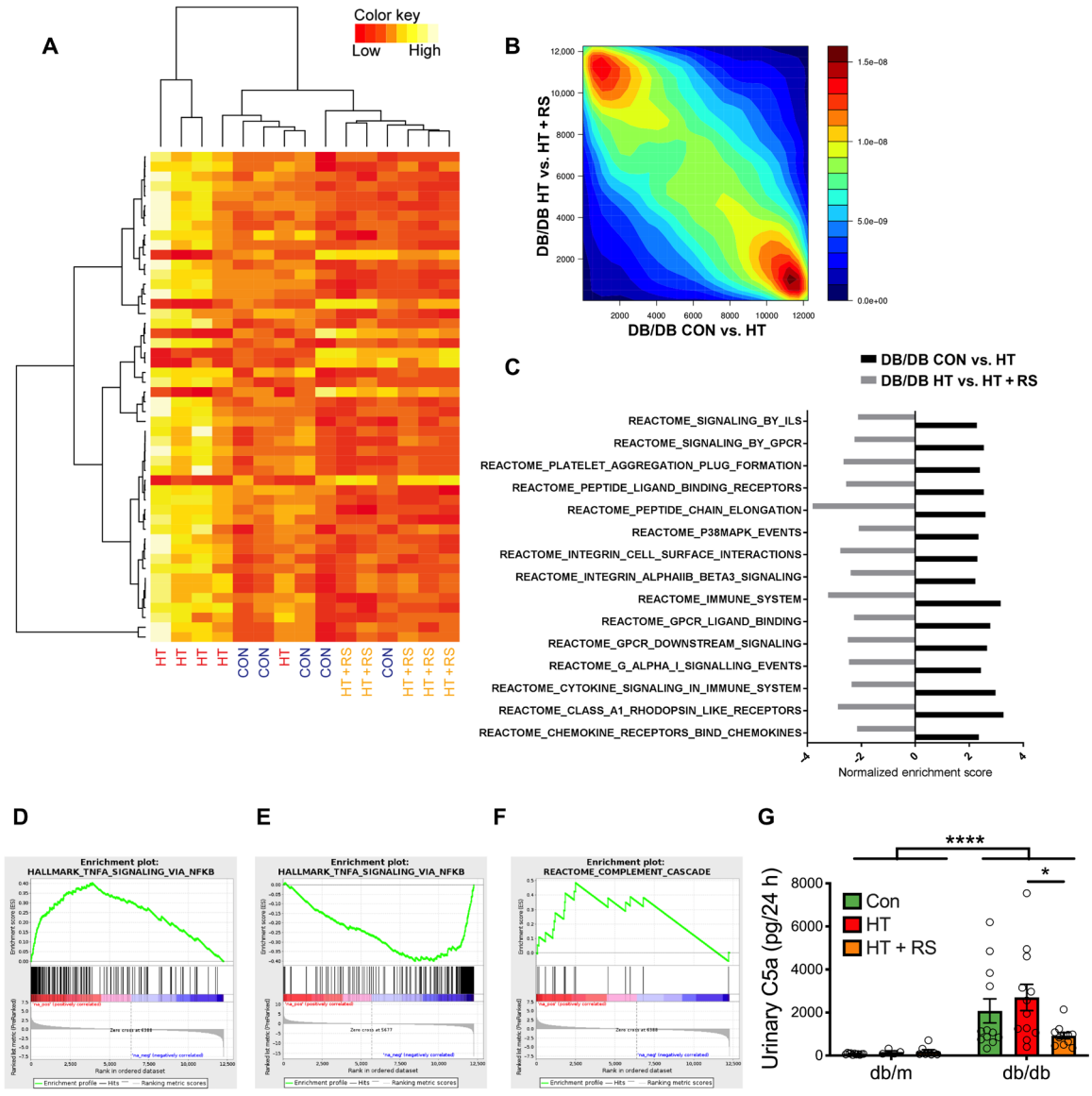

Fig. 6. In diabetic mice, resistant starch reverses immune and inflammatory pathways in the kidney. *Lepr*$^{db/db}$ (diabetic) and *db/m* (control) mice were fed an unbaked control diet (green), a heat-treated diet (red), or a heat-treated diet supplemented with resistant starch (high-amylose maize starch, orange) for 10 weeks, and transcriptomics (RNA sequencing) of the kidney was performed. (**A**) Heatmap showing hierarchical clustering of gene pathway (from MSigDB) expression patterns. (**B**) Rank-rank plot of expression differences due to diet in diabetic mice. Bottom right shows a cluster of genes (red) up-regulated in heat-treated diet and reversed by resistant starch. Top left cluster shows genes down-regulated by heat-treated diet and up-regulated by resistant starch. (**C**) Reactome pathway analysis shows that several immune signaling pathways are up-regulated by heat-treated diet feeding and down-regulated by resistant starch in *Lepr*$^{db/db}$ mice (FDR < 0.05). (**D**) GSEA plot illustrating up-regulation of TNF-α signaling via NF-κB with the heat-treated diet (NES = 5.97, FDR < 0.001). (**E**) GSEA plot illustrating down-regulation of TNF-α signaling via NF-κB with resistant starch supplementation (NES: −5.98, FDR < 0.001). (**F**) GSEA plot illustrating up-regulation of genes involved in the complement cascade with heat-treated diet feeding. (**G**) Twenty-four–hour urinary excretion of C5a. Data are means ± SEM. Dots represent individual rodents. **P* < 0.05, ***P* < 0.01, ****P* < 0.001, and *****P* < 0.0001. *P* values were determined by two-way ANOVA with Tukey's multiple comparisons test (G), *n* = 8 to 11 mice per group for urinary C5a analysis, *n* = 5 mice per group for renal transcriptome analysis.

Fig. 6D] and down-regulated in mice receiving a heat-treated diet supplemented with resistant starch (compared with mice fed a heat-treated diet, NES = −5.98, FDR < 0.001; Fig. 6E). Of note, and consistent with our earlier in vivo experimental models, a heat-treated diet was associated with an up-regulation of genes involved in the complement cascade (Fig. 6F). Interrogation of this pathway showed that *Lepr*$^{db/db}$ mice had an increase in complement C5a compared with nondiabetic mice, which was clearly suppressed with resistant starch supplementation (Fig. 6G). These findings show that in the context of diabetes, heat-treated diets trigger intestinal permeability and kidney damage, with up-regulation of local renal inflammatory pathways including complement, which can be attenuated with supplementation of fiber.

To explore whether inflammation might be localized to the kidney, we explored the liver as an alternate site of inflammation. Liver mRNAs for inflammatory cytokines and chemokines were unchanged with the heat-treated diet (fig. S7).

Heat-treated diets alter the cecal metabolome, with an up-regulation of amino acid metabolite pathways

These studies support the notion that chronic consumption of processed foods negatively affects renal health via changes in the gastrointestinal ecosystem. Fermentation of complex carbohydrates, proteins, and fats that reach the lower gastrointestinal tract by the gut microbiota results in the synthesis of a multitude of metabolites that can act both locally and systemically, and the digestibility of proteins by the host is influenced, in part, by food processing (*31*). We set out to identify the metabolites generated by the heat-treated diet–shaped gut microbiota in an attempt to ascertain whether these signals might represent known toxic metabolites that may be responsible for eliciting inflammation and renal injury. Thus, with this view, we investigated the mouse cecal metabolome. Using a supervised model, we observed differences among control (non–heat-treated), heat-treated, and heat-treated plus resistant starch diets, with notably the heat-treated plus resistant starch diet clustering near the non–heat-treated diet, and a clear heat-treated diet metabolome emerging (fig. S2A). The heat-treated diet was associated with an increase in metabolites in the phenylalanine, tryptophan, and tyrosine pathways (fig. S2B) and when resistant starch was added to a heat-treated diet, metabolic flux through these pathways was dampened (fig. S2C). Correlation analysis showed a positive correlation between these metabolites and the Firmicutes phyla, while Bacteroidetes (previously shown here to be reduced with a heat-treated diet) was negatively correlated (fig. S3).

To determine whether bacterial metabolites can directly promote complement activation, Caco-2 cells were exposed to two key metabolites shown to be up-regulated by the heat-treated diet: tyramine (Tyr) and 3-hydroxyphenylacetic acid (3-HPA). Incubation of Caco-2 cells with Tyr and 3-HPA up-regulated the expression of C3 and C5 (fig. S8, A to D), demonstrating that bacterial metabolites can activate complement and may provide a link between dietary AGEs and complement-mediated kidney damage.

DISCUSSION

It has become increasingly apparent that the modern Western diet, composed of processed foods rich in fat, sugar, and salt, significantly contributes to the obesity crisis, which also manifests a vast array of end-organ pathologies, such as nonalcoholic fatty liver disease, certain types of cancers, type 2 diabetes, and related macro- and microvascular diseases (*32*, *33*). The lifestyle of a substantial proportion of the populations of developed countries is characterized by a high intake of ready-to-eat foods such as breakfast cereals, biscuits, and snack foods, which have been highly heat processed. Food processing alters the chemical structure of foodstuffs and, in doing so, increases shelf-life, palatability, and sensory properties, inherently improving taste and potentially stimulating the reward centers in the brain, leading to overeating (*34*–*36*). While manufacturers may endeavor to limit the fat, sugar, and salt content of these products to meet healthy eating guidelines, these foods are often rich sources of AGEs. Here, we have established that the AGE component of processed foods is a mediator of microvascular disease risk.

Our studies have shown that chronic exposure of heat-treated diets hyperactivates a key component of innate immunity, the complement system, and that the proinflammatory complement end effector molecules C3a and C5a lead to kidney injury, which is consistent with a CKD phenotype. It has previously been postulated that AGEs and their precursors contribute to the pathogenesis of CKD, but the mechanisms have largely focused on endogenous pathways of formation, which accumulate in plasma during a decline in GFR and involve the AGE precursor methylglyoxal, and its endogenous detoxification system, the glyoxalase system (*37*). Here, we identify an alternative mechanism, whereby AGEs consumed as part of a heat-treated, processed food diet, promote intestinal permeability, and induce systemic innate immune complement activation, driving inflammation and kidney injury. Inhibition of the AGE pathway with alagebrium reverses the kidney injury phenotype and dampens complement activation due to a processed diet. Specific blockade of C5a signaling, using an orally active C5aR1 inhibitor, prevents renal injury, whereas genetic deletion of C3aR only leads to partial renoprotection. It is likely that blockade of C5a is more efficacious than C3a, because C5a is the most potent proinflammatory effector molecule of the complement pathway, being 50- to 100-fold more potent than C3a (*38*). C3a also plays a dual role, displaying inflammatory or anti-inflammatory actions under different conditions (*39*).

There is a consensus that low but persistent levels of systemic inflammation are common underlying features of chronic disease development (*40*), with a more recent interest in diet as a driver of inflammation (*41*). In the current studies, we observed that processed diets alter gut permeability in vivo, which occurred upstream of complement activation. Complement was not up-regulated at the level of the intestine as a result of eating a heat-treated diet, supporting the hypothesis that complement is activated distal to the gut (i.e., within the circulation). This was verified by in vitro studies using Caco-2 cells exposed to AGEs, where no activation of complement was seen. An activated complement cascade in the bloodstream gives rise to the production of the effector molecule C5a, which can bind to its receptor, C5aR1, on the kidney to induce inflammation and fibrosis, culminating in renal injury.

In a mouse model of diabetes, a high resistant starch fiber diet led to a redistribution of the gut commensal consortium, prevented impaired gut barrier function, and decreased the severity of renal injury via suppression of complement. These experimental findings are consistent with data from epidemiologic studies, which have shown that increased dietary fiber intake reduces all-cause mortality in patients with CKD (*42*). Results from this study provide mechanistic insight into the role of processed foods on inflammation and chronic disease risk, as well as a practical way in which the damage from overconsumption of highly processed diets could be mitigated. Given that some 30% of individuals in a healthy population may have undiagnosed mild renal insufficiency (*43*), overconsumption of thermally processed food may confer disease risk or exacerbate preexisting pathology.

Several limitations to this study exist. One limitation of this study is the absence of a reductionist approach that could have sought to identify the specific AGE moiety responsible for complement pathway activation and renal injury. Future studies could include individual AGEs enriched in diets or given via oral gavage, such as CML. However, because it is likely that there are multiple AGE moieties present in processed foodstuffs, the current study was designed to capture a "real world" approach by supplying a whole food matrix that had been heat-treated. In addition, although beyond the scope of the current study, future studies should endeavor to (i) identify the mechanism by which AGEs disrupt the intestinal epithelial barrier, (ii) determine whether bacterial metabolites

induce complement activation within the systemic circulation, and (iii) perform gut microbiome transfer studies from mice eating a highly processed diet to define a causal link between the gut microbiome in kidney injury.

Together, we provide evidence that chronic consumption of processed foods induces impaired intestinal barrier permeability and complement pathway activation and confers microvascular disease risk in rodents. Pharmacological inhibition of the proinflammatory C5a-C5aR1 axis prevents the deleterious effects of processed food intake. Last, we illustrate that a gut targeted dietary intervention limits the negative influence of the modern, processed diet, providing a practical way for food products to be better formulated to limit health consequences.

MATERIALS AND METHODS

Experimental design

Animals

All animal experiments were performed in accordance with guidelines from the Alfred Medical Research and Education Precinct (AMREP) Animal Ethics Committee and the National Health and Medical Research Council of Australia. All rodents were housed in a temperature-controlled environment, with a 12-hour light/dark cycle and access to chow (Specialty Feeds, Perth, WA, Australia) and water ad libitum. Male Sprague-Dawley rats were purchased from the Animal Resources Centre, Perth, Western Australia, Australia. C3aR$^{+/+}$ (wild type) and C3aR$^{-/-}$ mice (*44*) on a C57BL/6J genetic background (>12-generation backcross) were maintained at the University of Queensland's Biological Resources Animal Facilities under specific pathogen–free conditions.

For the C3aR$^{-/-}$ mouse and the rat studies, 6-week-old animals received either a control nonheated diet (unbaked AIN93G) or a thermally treated diet (AIN93G baked at 160°C for 1 hour; see below) for 24 weeks ad libitum. In addition to receiving thermally treated diets, a second cohort of rats was randomized to receive ALA (10 mg/kg per day) via oral gavage. A third cohort of rats received the thermally treated diet with daily oral gavage of PMX-53 (2 mg/kg per day).

For the diabetes study, 4-week-old male *db/m* and *Lepr*$^{db/db}$ mice heterozygous and homozygous for deletion of the *Lepr* gene (BKS.Cg-*Dock7*^{m}+/+ *Lepr*^{db}/J) were purchased from The Jackson Laboratory (Bar Harbor, ME) and allowed to acclimatize for 2 weeks before diet interventions at 6 to 7 weeks of age. Diets were provided ad libitum for 10 weeks. At the endpoint (week 8) of the diabetes study, fat mass and lean body mass were determined using a 4-in-1 EchoMRI body composition analyzer (Columbus Instruments, USA). In addition, mice were placed for 24 hours in a comprehensive laboratory animal monitoring system (CLAMS, OxyMax, USA) for the measurement of oxygen consumption, respiratory rate, and physical activity.

At week 24 of the rat studies and the C3aR$^{-/-}$ mouse study, and at week 9 of the *Lepr*$^{db/db}$ study, animals were housed in metabolic cages (Iffa Credo, L'Arbresle, France) for 24 hours for urine collection and measurement of food and water intake.

At the end of the intervention period, animals were anesthetized by an intraperitoneal injection of sodium pentobarbitone (rats, 50 mg/kg body weight; mice, 100 mg/kg body weight; Euthatal; Sigma-Aldrich, Castle Hill, Australia), followed by cardiac exsanguination. Blood was treated with sodium citrate (3.2% v/v) and centrifuged at 6000 rpm for 6 min, and plasma was frozen on dry ice and stored at −80°C. For the rat studies, the abdominal aorta was perfused with 0.1 M phosphate-buffered saline (PBS) for 1 to 2 min to remove circulating blood and kidneys were removed, sliced transversely, and either frozen in liquid nitrogen and stored at −80°C or postfixed overnight in neutral buffered formalin (10% v/v). Gut sections (ileum and jejunum) were also snap-frozen in liquid nitrogen and stored at −80°C. For the mouse studies, kidney sections were fixed in neutral buffered formalin (10% v/v). Kidney sections collected for RNA and protein analysis were snap-frozen in liquid nitrogen and stored at −80°C. Cecal contents were collected, snap-frozen in liquid nitrogen, and stored at −80°C.

Rodent diets

All diets were semipure formulations manufactured by Specialty Feeds (Western Australia, Australia). For the C3aR$^{-/-}$ mouse and rat studies, animals received either a control nonheated diet (unbaked AIN93G) or a thermally treated diet (AIN93G baked at 160°C for 1 hour; see method below) for 24 weeks ad libitum. For the diabetes study, *db/m* and *Lepr*$^{db/db}$ mice received either an unbaked control diet (SF15-021), a thermally treated diet (SF15-021, baked at 160°C for 1 hour), or a thermally treated diet supplemented with 25% resistant starch (SF15-015) for 10 weeks. The SF15-021 and SF15-015 diets were custom-formulated for this study and were matched for protein, fat, and caloric content.

AGE content of diets

The AGE content of thermally processed diets was determined using multiple methods. For determination of fructosamine in rodent chow, chow samples (30 μl, 10 mg/ml) were mixed with nitroblue tetrazolium (NBT) dye [180 μl, 0.5 mM in 100 mM carbonate buffer (pH 10.4)] and incubated at 37 ± 1°C in the dark. The absorbance was determined at 530 nm at 10 and 15 min using a multimode plate reader (Thermo Fisher Scientific, USA). The level of fructosamine was calculated from the standard curve generated by 1-deoxy-1-morpholinofructose (1-DMF) and expressed as μmol 1-DMF/g. Protein-bound CML, CEL, and methylglyoxal-derived hydroimidazolone-1 (MG-H1) were determined in rodent chow by MS as previously described (*45*). Briefly, powdered chow samples (20 mg) were mixed with borate buffer [0.2 M (pH 9.2), 200 μl] reduced with sodium borohydride (40 μl, 1 M in 0.1 M sodium hydroxide). After reduction, protein was precipitated using trichloroacetic acid (20%) and hydrolyzed in hydrochloric acid (6 M) for 24 hours at 100 ± 1°C. Samples were dried under nitrogen, reconstituted in 1% trifluoroacetic, and spiked with internal standard before solid-phase extraction. Sep-Pak (RP C_{18}) columns were used for solid-phase extraction, and the sample was eluted by trifluoroacetic acid (1% v/v in methanol 20% v/v). The samples were dried under nitrogen and reconstituted in 1 ml of methanol (20% v/v) before injection. Analysis of CML, CEL, and MG-H1 was performed using a Sciex QTRAP 6500^{+} liquid chromatography–mass spectrometer (Sciex, Framingham, MA, USA) and detected in electrospray ionization (ESI)–positive multiple reaction monitoring (MRM) mode. Derivatives were separated on a reversed-phase C_{18} column (Phenomenex Synergi Hydro-RP; 4-μm particle size, 80-Å pore size, 150 mm × 4.6 mm; Phenomenex, Torrance, CA, USA) with a linear gradient of 0.1% formic acid (FA) and acetonitrile. The sample injection was 1 μl with a flow rate of 0.4 ml/min over 6 min. The MRM transitions used were Lys (147.4>83.9), CML (205.1>84), CEL (219.2>130), MG-H1 (229.2>116.1), [$^{2}H_{2}$]-Lys (151.2>87.9), [$^{2}H_{2}$]-CML (207.1>129.9) [$^{4}H_{2}$]-CEL (222.9>134.2), and [3H2]-MG-H1 (232.2>116.1). A standard

calibration curve was prepared by a plot of analyte peak area divided by internal standard peak area (area ratio) against concentration (amount ratio) and values expressed as nmol/g sample or mmol/mol Lys.

In addition, CML content was determined in rodent chow in triplicate by HPLC as previously described (*46*). CML concentrations in rodent chow were standardized to protein-bound serine (Ser) concentrations in each sample to compensate for any losses during sample processing. To determine any losses in heat-labile vitamins, thiamine content of the unbaked and baked rodent chow was measured using *Lactobacillus fermentum* [American Type Culture Collection (ATCC) 9338] and thiamine assay broth (Difco, Detroit, MI, USA).

Determination of renal injury

Urinary albumin was determined by enzyme-linked immunosorbent assay (ELISA; Bethyl Laboratories, Montgomery, TX, USA), specific for mice (E90-124A) or rats (E110-125) as appropriate. Urinary kidney injury molecule-1 (KIM-1) was measured by ELISA specific for rats (Bioassay Works, Ijamsville, MD) or mouse (USCN Life Sciences, Wuhan, China). Albumin and KIM-1 concentrations were multiplied by 24-hour urine volume to obtain the albumin excretion rate. For the rat studies and the C3aR$^{-/-}$ mouse study, urinary and plasma creatinine was determined by high-performance liquid chromatography (HPLC) (Agilent HP1100 system, Hewlett Packard, Germany). For the diabetes study, urinary and plasma creatinine concentrations were measured using a commercially available creatinine assay kit (Roche Diagnostics, catalog no. 03263991190) on a Cobas Integra 400 Plus autoanalyzer (Roche Diagnostics). Urinary creatinine was determined by multiplication of the urinary creatinine concentration by the 24-hour urine volume for each rodent. Creatinine clearance was estimated as a ratio between 24-hour urinary creatinine and plasma creatinine concentration, expressed as ml min^{-1} m^{-2} body surface area, as reported previously (*47*). Plasma cystatin C was determined using a commercially available kit according to the manufacturer's instructions (BioVendor, Czech Republic).

Renal histopathology

GSI was evaluated in a blinded manner by a semiquantitative method. Paraffin-embedded left kidney was sectioned (3 μm) and stained with periodic acid–Schiff (PAS) reagent. Sections were observed at a magnification of ×400 under a light microscope (Analysis Imaging System, AIS, Imaging Research, St. Catharines, Ontario, Canada). Twenty glomeruli per section were graded according to the severity of glomerular damage including mesangial matrix expansion and/or hyalinosis with focal adhesions, true glomerular tuft occlusion, sclerosis, and capillary dilation. The degree of sclerosis in each glomerulus was graded subjectively on a scale of 0 to 4: grade 0, normal; grade 1, sclerotic area up to 25% (minimal); grade 2, sclerotic area 26 to 50% (moderate); grade 3, sclerotic area 51 to 75%; and grade 4, sclerotic area 76 to 100% (severe). The GSI was then calculated using the following formula: GSI = $(1 \times n1) + (2 \times n2) + (3 \times n3) + (4 \times n4)/(n0 + n1 + n2 + n3 + n4)$, where nx is the number of glomeruli in each grade of GSI.

Tubulointerstitial area (TIA) was assessed in a blinded manner by a point-counting technique in paraffin-embedded PAS-stained sections at a magnification of ×200. In each field, 81 points were counted on an eyepiece graticule with 9 equidistant grid lines. A total of 10 corticomedullary fields per kidney section were counted. Percent fractional area (FA), corresponding to the percentage of TIA in the total area counted for that section, was calculated using the formula %FA = (number of tubulointerstitial grid intersections/total number of grid intersections) × 100.

Immunohistochemistry

C5aR protein was determined on formalin-fixed paraffin-embedded sections by immunohistochemistry using a rabbit anti-C5aR1 polyclonal antibody (Novus Biologicals #NB100-92153). Rat kidney paraffin sections were dewaxed and rehydrated. Endogenous peroxidases were quenched with 3% hydrogen peroxide/tris-buffered saline (TBS) followed by blocking with Superblock Blocking Buffer (Thermo Fisher Scientific, Australia). The rabbit anti-C5aR1 primary antibody was diluted 1:250 in TBS, and sections were incubated overnight at 4°C. After washing, sections were incubated with biotinylated secondary antibody (goat anti-rabbit immunoglobulin G; Vector Laboratories, Burlingame, CA, USA; 1:500 in TBS) for 10 min and then avidin-biotin complex (ABC; Vectastain Elite ABC kit, Vector Laboratories Inc., Burlingame, CA, USA) for 30 min. C5aR staining was visualized by DAB (3,3′-diaminobenzidine tetrahydrochloride; Sigma-Aldrich, St. Louis, MO, USA). Sections were counterstained with hematoxylin, dehydrated, and mounted in DPX (Fluka Chemie AG, Buchs, Switzerland). Quantitation of immunohistochemistry was performed by computer-aided densitometry (Image-Pro Plus 6.0, Media Cybernetics Inc., Bethesda, MD, USA).

Renal cortical fractionation

The renal cortex was fractionated into cellular compartments via differential ultracentrifugation. One hundred milligrams of kidney cortex was homogenized in an isolation buffer containing 20 mM Hepes, 1 mM EGTA, 210 mM mannitol, and 70 mM sucrose (pH 7.2). Renal cortical homogenates were centrifuged at 1000*g* for 10 min at 4°C. The pellet, containing the nuclear fraction, was resuspended in buffer [10 mM Hepes, 10 mM KCl, 0.1 mM EDTA, and 0.1 mM EGTA (pH 7.9)] and centrifuged at 7000*g* for 30 s at 4°C. The resulting pellet was resuspended in buffer [20 mM Hepes, 400 mM NaCl, 1 mM EDTA, 1 mM EGTA (pH 7.9)], and suspensions were incubated on ice for 20 min, with subsequent centrifugation at 10,000*g* for 30 min at 4°C. The supernatant contained the nuclear fraction. The supernatant from the initial renal cortical homogenate spin was centrifuged at 10,000*g* for 20 min at 4°C to obtain the mitochondrial pellet. The supernatant was further centrifuged at 100,000*g* for 1 hour at 4°C to yield the membrane fraction in the pellet and the cytosol in the supernatant. The membranous pellet was then resuspended in isolation buffer (as described above) containing 1% Triton X-100 and centrifuged again at 100,000*g* for 1 hour at 4°C, and the supernatant was collected as the membranous fraction. Total protein was determined by the bicinchoninic acid method according to the manufacturer's instructions (Pierce, Rockford, IL, USA).

VEGF determination

VEGF was measured in renal cortical cytosolic fractions using a commercially available kit (Quantikine Rat VEGF Immunoassay, R&D Systems, Minneapolis, MN, USA) according to the manufacturer's instructions.

TGF-β measurement

TGF-β1 was measured in renal cortical membrane fractions using the Promega TGF-β1 Emax ImmunoAssay System (Promega, Madison, WI, USA). Active TGF-β1 was measured by diluting samples 1:5 with PBS and then adjusting the pH to 3.0 with 1 M HCl. Samples were incubated for 15 min at room temperature and then neutralized with 1 M NaOH. TGF-β1 was determined according to the manufacturer's instructions.

Nitrotyrosine

Nitrotyrosine was determined in renal cortical mitochondrial fractions by ELISA (Oxis Research, Portland, OR, USA) according to the manufacturer's instructions.

NADH-driven superoxide radical generation

Kidneys were rapidly excised, placed in oxygen-saturated Krebs buffer [containing 118 mM NaCl, 4.7 mM KCl, 1.2 mM $MgSO_4.7H_2O$, 1.2 mM KH_2PO_4, 11 mM D-glucose, 0.03 mM EDTA, and 2.5 mM $CaCl_2$ (pH 7.4)], and dissected into ~1-mm segments. The rate of superoxide anion formation was determined by lucigenin (bis-*N*-methylacridinium nitrate; Sigma Chemical Company). Briefly, 100 μl of substrate [125 μM NADH (reduced form of nicotinamide adenine dinucleotide)] and 100 μM rotenone (mitochondrial complex I inhibitor) were added to fresh tissue slices (in triplicate). The plate was warmed in the luminometer for 60 min at 37°C before the addition of 3.8 μM lucigenin. Chemiluminescence was monitored every 6 min for 60 min, and the integral over this period was expressed as relative light units (RLUs). Results were normalized to 10-mg dry tissue weight.

Complement and inflammatory markers

Plasma MCP-1 was determined using a commercially available ELISA kit (R&D Systems, USA) according to the manufacturer's instructions. An ELISA was used for the determination of urinary C5a (mouse: DY2150 DuoSet C5a ELISA, R&D Systems; rat: USCN Life Sciences, China) and urinary C3a (USCN Life Sciences, China). Urinary 15-isoprostane F_{2t} was measured by a commercially available ELISA kit (Oxford Biomedical Research, MI, USA). All concentrations were multiplied by total urine volume over 24 hours to obtain the daily excretion rate.

SDS–polyacrylamide gel electrophoresis, in-gel tryptic digestion, and MS

Rat serum samples were diluted 1:100 in Milli-Q water and reduced using β-mercaptoethanol (80°C, 5 min). After quenching on ice, samples were separated using SDS–polyacrylamide gel electrophoresis (SDS-PAGE) (8% gel) under standard conditions. The gel was stained with Coomassie blue dye, destained, and visualized on an Odyssey imaging system (Li-Cor Biosciences, Lincoln, NE, USA). Gel bands were manually excised and destained with a solution of 50 mM ammonium bicarbonate and 50% acetonitrile. The gel pieces were washed and dehydrated with alternating washing cycles of 50 mM ammonium bicarbonate and acetonitrile. After complete dehydration of the gel piece, it was rehydrated with a solution containing 0.5 μg of trypsin (Promega Corp., Madison, WI, USA) in 20 mM ammonium bicarbonate. The gel pieces were incubated at 37°C overnight and sonicated for 10 min before analysis. MALDI-TOF/TOF was performed as previously described (*48*). Digest samples were co-spotted onto the MALDI target plate with Matrix solution of α-cyano-4-hydroxycinnamic acid (10 mg/ml) (Laser BioLabs, Sophia-Antipolis, France) in 50% acetonitrile/0.1% trifluoroacetic acid. The samples were analyzed on an Applied Biosystems (Foster City, CA, USA) 4700 Proteomics Analyzer MALDI-TOF/TOF in reflectron mode with a mass range of 800 to 3500 Da, focus mass of 1400 Da at 1500 shots per spectra. The 4700 Series Explorer software (version 3.0) automatically selected the 15 most intense peptides as precursor masses for MS/MS analysis and acquired in the order of decreasing intensity. MS/MS analysis was carried out in reflector mode with a relative precursor mass window of 50 resolution with metastable ion suppression on and spectra summed 2500 shots/spectrum. Peptide mass fingerprinting and MS/MS data were compiled by the GPS explorer software version 3 (build 311) (Applied Biosystems, Foster City, CA, USA) and searched against the National Center for Biotechnology Information (NCBI) nonredundant and Swiss-Prot databases using the MASCOT search engine (version 1.9, Matrix Science Inc., London, UK) with all taxonomy selected. The following search parameters were used: missed cleavages, 1; peptide mass tolerance, ±50 ppm (parts per million); peptide fragment tolerance, ±0.1 Da; peptide charge, 1+; fixed modifications, carbamidomethyl; variable modification, oxidation (Met).

RNA extraction and quantitative polymerase chain reaction

RNA extracted from gut sections and kidney cortex was used to synthesize complementary DNA (cDNA) for reverse transcription polymerase chain reaction (RT-PCR), as previously described (*49*). In brief, TRIzol Reagent (Life Technologies) was used to extract RNA, which was reverse-transcribed using the SuperScript First-Strand Synthesis System (Life Technologies BRL, Grand Island, NY). Real-time PCR was performed using SYBR Green (Applied Biosystems, Mulgrave, VIC, Australia) or TaqMan PCR mix and analyzed with an ABI Prism 7500 sequence detector (Applied Biosystems 7500 Real-Time PCR Systems, California, USA) for rat studies or the QuantStudio 3 or 5 Real-Time PCR System (Thermo Fisher Scientific) for the diabetes mouse study. Results were normalized to 18*S* rRNA for kidney samples or β-actin for gut samples. Results are expressed as fold change relative to control.

Intestinal permeability

Plasma endotoxin concentration was determined using a commercially available kit based on a Limulus amoebocyte lysate (LAL kit endpoint, QCL-1000; Lonza, Walkersville, USA) according to the manufacturer's instructions. At week 10 of the diabetes study, intestinal permeability was assessed in vivo using the previously described FITC-conjugated dextran (FITC-labeled dextran) technique. Mice were fasted for 6 hours and gavaged with dextran-FITC (500 mg/kg body weight) (Sigma-Aldrich) diluted in PBS. Approximately 120 μl of blood was collected 1 hour after gavage via tail vein bleed and centrifuged at 6000 rpm for 6 min, and fluorescence was determined in plasma using a fluorescence spectrophotometer at excitation at 490 nm and emission at 520 nm, and FITC-dextran concentration was calculated using an FITC-dextran standard curve.

Oral glucose tolerance test

At week 9 of the diabetic study, an OGTT was performed. Mice were fasted for 6 hours and gavaged orally with body weight glucose (2 g/kg). Blood was collected at baseline, 15 min, and 60 min and centrifuged at 6000 rpm for 6 min, and plasma was separated and stored at −80°C. Glucose levels were determined using a glucose colorimetric assay kit (Cayman, Ann Arbor, MI, USA), and insulin concentrations were determined via ELISA (Alpco, Salem, NH, USA). HOMA-IR was calculated to indicate insulin sensitivity. Glycated hemoglobin was measured in blood collected at cull with a Cobas Integra 400 autoanalyzer (Roche Diagnostics Corporation, USA).

Microbiome

Cecal contents were collected and snap-frozen in liquid nitrogen and stored at −80°C. DNA extraction and sequencing were completed at the Australian Centre for Ecogenomics (Queensland, Australia). Paired-end reads of the V3-V4 region of the 16*S* rRNA gene were sequenced on the Illumina MiSeq platform using primer pair Bac_SSU_341F-806wR. Reads were trimmed using skewer version 0.2.2, and microbial identity was assigned using QIIME 1.9.1, using open reference operational taxonomic unit (OTU) picking to greengenes (version 13_8) with an OTU cutoff of 97%. There was an average sequence depth of 42,093 and 35,103 reads for the C57BL6 and db/db mouse experiments, respectively. All samples were included in the analyses. Cladograms were created using the LefSe tool of the Huttenhower laboratory, with an α value for factorial Kruskal-Wallis test among classes set to 0.05 and an LDA threshold score of 4.0 (*26*).

Cecal metabolome

An untargeted metabolomics analysis was conducted by Metabolon (Morrisville, NC, USA). Preparation of samples was performed using an automated MicroLab STAR system (Hamilton Company, NV, USA). Proteins were precipitated with methanol under vigorous shaking for 2 min using GenoGrinder 2000 (Glen Mills, NJ, USA) and subsequent centrifugation. The extract was divided into four fractions, with one for analysis by reversed-phase (RP)/ultraperformance liquid chromatography (UPLC)– MS/MS with negative ion mode ESI, one for analysis by hydrophilic interaction liquid chromatography (HILIC)/UPLC-MS/MS with negative ion mode ESI, and two being analyzed by RP/UPLC-MS/MS methods with positive ion mode ESI. Organic solvents were removed using a TurboVap (Zymark, Hopkinton, MA, USA). A Waters ACQUITY UPLC and a Thermo Fisher Scientific Q-Exactive high resolution/accurate mass spectrometer interfaced with a heated ESI source and an Orbitrap mass analyzer operated at 35,000 mass resolution were used for all methods. The sample extract was dried and then reconstituted in solvents compatible to each of the four methods. Each reconstitution solvent contained a series of standards at fixed concentrations to ensure injection and chromatographic consistency. One aliquot was analyzed using acidic positive ion conditions, chromatographically optimized for more hydrophilic compounds. In this method, the extract was gradient-eluted from a C18 column (Waters UPLC BEH C18 2.1 × 100 mm, 1.7 μm) using water and methanol containing 0.05% perfluoropentanoic acid (PFPA) and 0.1% FA. Another aliquot was also analyzed using acidic positive ion conditions; however, it was chromatographically optimized for more hydrophobic compounds. In this method, the extract was gradient-eluted from the same aforementioned C18 column using methanol, acetonitrile, water, 0.05% PFPA, and 0.01% FA and was operated at an overall higher organic content. Another aliquot was analyzed using basic negative ion optimized conditions using a separate dedicated C18 column. The basic extracts were gradient-eluted from the column using methanol and water with 6.5 mM ammonium bicarbonate at pH 8. The fourth aliquot was analyzed via negative ionization following elution from a HILIC column (Waters UPLC BEH Amide 2.1 × 150 mm, 1.7 μm) using a gradient consisting of water and acetonitrile with 10 mM ammonium formate (pH 10.8). The MS analysis alternated between MS and data-dependent MSn scans using dynamic exclusion. The scan range varied slightly between methods but covered 70 to 1000 *m/z* (mass/charge ratio). Raw data were extracted, peak-identified, and quality control (QC)–processed using Metabolon's hardware and software. Compounds were identified by comparison to a library based on authenticated standards that contains the retention time/index (RI), *m/z*, and chromatographic data (including MS/MS spectral data) on all molecules present in the library. Furthermore, biochemical identifications are based on three criteria: retention index within a narrow RI window of the proposed identification, accurate mass match to the library ±10 ppm, and the MS/MS forward and reverse scores between the experimental data and authentic standards. The MS/MS scores are based on a comparison of the ions present in the experimental spectrum to the ions present in the library spectrum. For data visualization, enrichment maps were created using Cytoscape version 2.8.3 (*50*) and using the MetaboLync Pathway Visualizations plugin (version 1.1.10, Metabolon Inc., Research Triangle Park, NC, USA).

RNA sequencing

RNA was isolated from TRIzol homogenates using the Direct-zol RNA MiniPrep Kit by Zymo Research. RNA quality was assessed with a MultiNA bioanalyzer. Two hundred nanograms of total RNA underwent rRNA depletion using the NEBNext rRNA Depletion Kit followed by library construction using NEBNext Ultra Directional RNA Library Prep Kit for Illumina (both from NEB, USA). Library QC was performed with the MultiNA Bioanalyzer (Shimadzu, Japan) and then pooled to equimolar concentration. Pooled libraries underwent Illumina single-read sequencing at the Australian Genome Research Facility (AGRF), Melbourne using HiSeq v4 reagents to generate 100–base pair reads. Reads were trimmed for quality using a minimum phred value of 20 and minimum length of 18 using FastX Toolkit (*51*). Reads were mapped with STAR (*52*) to the mouse genome downloaded from Ensembl (GRCm38). rRNA carryover was quantified by mapping reads to 5*S*, 18*S*, 28*S*, and Rs5-8s1 sequenced with BWA aln (*53*). FeatureCounts (*54*) was used to count reads mapped to gene bodies on the correct strand with a minimum mapping quality of 20 using Ensembl genome annotation (Mus musculus.GRCm38.85.gtf). The resulting count matrix underwent differential analysis with the EdgeR package (*55*). MA plots were generated in R. Genes were ranked from most up-regulated to most down-regulated by multiplying the sign of the $\log_2$ fold change by the inverse of the *P* value. This preranked list was used for pathway analysis using GSEA (*56*). Gene sets used included REACTOME (*57*), MSigDB (*58*), and Encode TFBS (*59*).

Cell culture experiments

Cell culture experiments were conducted using the Caco-2 human colorectal adenocarcinoma epithelial cell line (ATCC, HTB-37). Cells were cultured in Dulbecco's modified Eagle's medium (Gibco) supplemented with 5.5 mM glucose (Sigma-Aldrich), 10% (v/v) fetal bovine serum, 1% (v/v) sodium pyruvate (Sigma-Aldrich), 1% (v/v) L-glutamine, and 1% (v/v) penicillin/streptomycin. When near confluence, cells were detached using trypsin and seeded at a density of 1×10^5 cells/ml into 48-well plates for gene expression analysis and at a density of 5×10^5 cells/ml into six-well plates for cell culture supernatant analyses. Cells were cultured for 2 to 3 days, and when cells had reached 80 to 90% confluence, experimental agents were added. Experiment 1: (i) Control human serum albumin (HSA) (100 μg/ml) or (ii) AGE-modified HSA (AGE-HSA) (100 μg/ml). AGE-HSA was prepared as previously described (*60*). Experiment 2: (i) Control (media only), (ii) 100 μM tyramine (Sigma-Aldrich, catalog no.: H50004), or (iii) 2 mM 3-HPA (Sigma-Aldrich, catalog no.: H49901). Cells were treated with experimental agents for a period of 24 hours. For real-time PCR, cells were lysed and treated with deoxyribonuclease. cDNA synthesis from RNA was completed using reverse transcriptase (sensiFAST) in the presence of a ribonuclease inhibitor (New England BioLabs). Real-time PCR was performed using SYBR Green (Applied Biosystems, Mulgrave, Victoria, Australia) or TaqMan PCR mix and analyzed using the QuantStudio 5 Real Time PCR System (Thermo Fisher Scientific). Gene expression was normalized to 18*S* mRNA and reported as fold change relative to the control group. Following treatment, the supernatant from the six-well plate experiments was collected. C5a in the supernatant was measured by ELISA (BD Biosciences, catalog no.: 557965).

Statistics

The data are expressed either as scatterplots of the data showing the mean or as means ± SEM. Statistical analyses were performed using GraphPad Prism version 7.0 (GraphPad Software, La Jolla, CA, USA). For the animal studies, comparisons between two groups were performed using unpaired two-tailed Student's *t* test. If data

were nonparametric, a Mann Whitney test was used. For comparison between multiple groups, one-way analysis of variance (ANOVA) with Tukey's post hoc test was performed. Data not normally distributed were analyzed after logarithmic transformation. For studies using mice of different genotypes (C3aR$^{-/-}$, *Lepr*$^{db/db}$), a two-way ANOVA with Sidak's post hoc test was performed. A P value less than 0.05 was considered significant.

SUPPLEMENTARY MATERIALS

Supplementary material for this article is available at http://advances.sciencemag.org/cgi/content/full/7/14/eabe4841/DC1

View/request a protocol for this paper from *Bio-protocol*.

REFERENCES AND NOTES

1. M. K. Zinöcker, I. A. Lindseth, The Western diet–microbiome-host interaction and its role in metabolic disease. *Nutrients* **10**, 365 (2018).
2. C. A. Monteiro, J.-C. Moubarac, G. Cannon, S. W. Ng, B. Popkin, Ultra-processed products are becoming dominant in the global food system. *Obes. Rev.* **14** (suppl. 2), 21–28 (2013).
3. M. Bluher, Obesity: Global epidemiology and pathogenesis. *Nat. Rev. Endocrinol.* **15**, 288–298 (2019).
4. K. Ogurtsova, J. D. da Rocha Fernandes, Y. Huang, U. Linnenkamp, L. Guariguata, N. H. Cho, D. Cavan, J. E. Shaw, L. E. Makaroff, IDF Diabetes Atlas: Global estimates for the prevalence of diabetes for 2015 and 2040. *Diabetes Res. Clin. Pract.* **128**, 40–50 (2017).
5. N. R. Hill, S. T. Fatoba, J. L. Oke, J. A. Hirst, C. A. O'Callaghan, D. S. Lasserson, F. D. Hobbs, Global prevalence of chronic kidney disease—A systematic review and meta-analysis. *PLOS ONE* **11**, e0158765 (2016).
6. A. S. Go, G. M. Chertow, D. Fan, C. E. McCulloch, C. Y. Hsu, Chronic kidney disease and the risks of death, cardiovascular events, and hospitalization. *N. Engl. J. Med.* **351**, 1296–1305 (2004).
7. M. Hellwig, T. Henle, Baking, ageing, diabetes: A short history of the Maillard reaction. *Angew. Chem. Int. Ed. Engl.* **53**, 10316–10329 (2014).
8. M. W. Poulsen, R. V. Hedegaard, J. M. Andersen, B. de Courten, S. Bügel, J. Nielsen, L. H. Skibsted, L. O. Dragsted, Advanced glycation endproducts in food and their effects on health. *Food Chem. Toxicol.* **60**, 10–37 (2013).
9. J. L. J. M. Scheijen, E. Clevers, L. Engelen, P. C. Dagnelie, F. Brouns, C. D. A. Stehouwer, C. G. Schalkwijk, Analysis of advanced glycation endproducts in selected food items by ultra-performance liquid chromatography tandem mass spectrometry: Presentation of a dietary AGE database. *Food Chem.* **190**, 1145–1150 (2016).
10. J. Degen, M. Hellwig, T. Henle, 1,2-Dicarbonyl compounds in commonly consumed foods. *J. Agric. Food Chem.* **60**, 7071–7079 (2012).
11. M. A. van Boekel, Formation of flavour compounds in the Maillard reaction. *Biotechnol. Adv.* **24**, 230–233 (2006).
12. N. Aljahdali, F. Carbonero, Impact of Maillard reaction products on nutrition and health: Current knowledge and need to understand their fate in the human digestive system. *Crit. Rev. Food Sci. Nutr.* **59**, 474–487 (2019).
13. F. J. Tessier, C. Niquet-Léridon, P. Jacolot, C. Jouquand, M. Genin, A.-M. Schmidt, N. Grossin, E. Boulanger, Quantitative assessment of organ distribution of dietary protein-bound 13C-labeled Nε-carboxymethyllysine after a chronic oral exposure in mice. *Mol. Nutr. Food Res.* **60**, 2446–2456 (2016).
14. T. P. N. Bui, A. D. Troise, V. Fogliano, W. M. de Vos, Anaerobic degradation of *N*-ε-Carboxymethyllysine, a major glycation end-product, by human intestinal bacteria. *J. Agric. Food Chem.* **67**, 6594–6602 (2019).
15. M. Hellwig, D. Bunzel, M. Huch, C. M. Franz, S. E. Kulling, T. Henle, Stability of individual maillard reaction products in the presence of the human colonic microbiota. *J. Agric. Food Chem.* **63**, 6723–6730 (2015).
16. T. Fiolet, B. Srour, L. Sellem, E. Kesse-Guyot, B. Alles, C. Mejean, M. Deschasaux, P. Fassier, P. Latino-Martel, M. Beslay, S. Hercberg, C. Lavalette, C. A. Monteiro, C. Julia, M. Touvier, Consumption of ultra-processed foods and cancer risk: Results from NutriNet-Sante prospective cohort. *BMJ* **360**, k322 (2018).
17. A. Rico-Campà, M. A. Martínez-González, I. Alvarez-Alvarez, R. D. Mendonca, C. de la Fuente-Arrillaga, C. Gómez-Donoso, M. Bes-Rastrollo, Association between consumption of ultra-processed foods and all cause mortality: SUN prospective cohort study. *BMJ* **365**, l1949 (2019).
18. L. Schnabel, E. Kesse-Guyot, B. Alles, M. Touvier, B. Srour, S. Hercberg, C. Buscail, C. Julia, Association between ultraprocessed food consumption and risk of mortality among middle-aged adults in France. *JAMA Intern. Med.* **179**, 490–498 (2019).
19. X. M. Meng, D. J. Nikolic-Paterson, H. Y. Lan, TGF-β: The master regulator of fibrosis. *Nat. Rev. Nephrol.* **12**, 325–338 (2016).
20. D. M. Okamura, S. Pennathur, The balance of powers: Redox regulation of fibrogenic pathways in kidney injury. *Redox Biol.* **6**, 495–504 (2015).
21. M. J. Walport, Complement. First of two parts. *N. Engl. J. Med.* **344**, 1058–1066 (2001).
22. O. A. Hawksworth, X. X. Li, L. G. Coulthard, E. J. Wolvetang, T. M. Woodruff, New concepts on the therapeutic control of complement anaphylatoxin receptors. *Mol. Immunol.* **89**, 36–43 (2017).
23. T. M. Woodruff, K. S. Nandakumar, F. Tedesco, Inhibiting the C5-C5a receptor axis. *Mol. Immunol.* **48**, 1631–1642 (2011).
24. C. A. Thaiss, M. Levy, I. Grosheva, D. Zheng, E. Soffer, E. Blacher, S. Braverman, A. C. Tengeler, O. Barak, M. Elazar, R. Ben-Zeev, D. Lehavi-Regev, M. N. Katz, M. Pevsner-Fischer, A. Gertler, Z. Halpern, A. Harmelin, S. Aamar, P. Serradas, A. Grosfeld, H. Shapiro, B. Geiger, E. Elinav, Hyperglycemia drives intestinal barrier dysfunction and risk for enteric infection. *Science* **359**, 1376–1383 (2018).
25. L. A. David, C. F. Maurice, R. N. Carmody, D. B. Gootenberg, J. E. Button, B. E. Wolfe, A. V. Ling, A. S. Devlin, Y. Varma, M. A. Fischbach, S. B. Biddinger, R. J. Dutton, P. J. Turnbaugh, Diet rapidly and reproducibly alters the human gut microbiome. *Nature* **505**, 559–563 (2014).
26. N. Segata, J. Izard, L. Waldron, D. Gevers, L. Miropolsky, W. S. Garrett, C. Huttenhower, Metagenomic biomarker discovery and explanation. *Genome Biol.* **12**, R60 (2011).
27. D. P. Belobrajdic, A. R. Bird, M. A. Conlon, B. A. Williams, S. Kang, C. S. McSweeney, D. Zhang, W. L. Bryden, M. J. Gidley, D. L. Topping, An arabinoxylan-rich fraction from wheat enhances caecal fermentation and protects colonocyte DNA against diet-induced damage in pigs. *Br. J. Nutr.* **107**, 1274–1282 (2012).
28. M. Snelson, N. J. Kellow, M. T. Coughlan, Modulation of the gut microbiota by resistant starch as a treatment of chronic kidney diseases: Evidence of efficacy and mechanistic insights. *Adv. Nutr.* **10**, 303–320 (2019).
29. A. Trompette, E. S. Gollwitzer, K. Yadava, A. K. Sichelstiel, N. Sprenger, C. Ngom-Bru, C. Blanchard, T. Junt, L. P. Nicod, N. L. Harris, B. J. Marsland, Gut microbiota metabolism of dietary fiber influences allergic airway disease and hematopoiesis. *Nat. Med.* **20**, 159–166 (2014).
30. J. Wong, Y. M. Piceno, T. Z. DeSantis, M. Pahl, G. L. Andersen, N. D. Vaziri, Expansion of urease- and uricase-containing, indole- and p-cresol-forming and contraction of short-chain fatty acid-producing intestinal microbiota in ESRD. *Am. J. Nephrol.* **39**, 230–237 (2014).
31. C. K. Yao, J. G. Muir, P. R. Gibson, Review article: Insights into colonic protein fermentation, its modulation and potential health implications. *Aliment. Pharmacol. Ther.* **43**, 181–196 (2016).
32. L. Cordain, S. B. Eaton, A. Sebastian, N. Mann, S. Lindeberg, B. A. Watkins, J. H. O'Keefe, J. Brand-Miller, Origins and evolution of the Western diet: Health implications for the 21st century. *Am. J. Clin. Nutr.* **81**, 341–354 (2005).
33. A. Odermatt, The Western-style diet: A major risk factor for impaired kidney function and chronic kidney disease. *Am. J. Physiol. Renal Physiol.* **301**, F919–F931 (2011).
34. H. R. Berthoud, The neurobiology of food intake in an obesogenic environment. *Proc. Nutr. Soc.* **71**, 478–487 (2012).
35. M. R. Lowe, M. L. Butryn, Hedonic hunger: A new dimension of appetite? *Physiol. Behav.* **91**, 432–439 (2007).
36. T. L. Fazzino, K. Rohde, D. K. Sullivan, Hyper-palatable foods: Development of a quantitative definition and application to the US food system database. *Obesity (Silver Spring)* **27**, 1761–1768 (2019).
37. N. Rabbani, P. J. Thornalley, Advanced glycation end products in the pathogenesis of chronic kidney disease. *Kidney Int.* **93**, 803–813 (2018).
38. M. U. Ehrengruber, T. Geiser, D. A. Deranleau, Activation of human neutrophils by C3a and C5A. Comparison of the effects on shape changes, chemotaxis, secretion, and respiratory burst. *FEBS Lett.* **346**, 181–184 (1994).
39. L. G. Coulthard, T. M. Woodruff, Is the complement activation product C3a a proinflammatory molecule? Re-evaluating the evidence and the myth. *J. Immunol.* **194**, 3542–3548 (2015).
40. G. S. Hotamisligil, Inflammation and metabolic disorders. *Nature* **444**, 860–867 (2006).
41. C. M. Phillips, L. W. Chen, B. Heude, J. Y. Bernard, N. C. Harvey, L. Duijts, S. M. Mensink-Bout, K. Polanska, G. Mancano, M. Suderman, N. Shivappa, J. R. Hebert, Dietary inflammatory index and non-communicable disease risk: A narrative review. *Nutrients* **11**, (2019).
42. V. M. Krishnamurthy, G. Wei, B. C. Baird, M. Murtaugh, M. B. Chonchol, K. L. Raphael, T. Greene, S. Beddhu, High dietary fiber intake is associated with decreased inflammation and all-cause mortality in patients with chronic kidney disease. *Kidney Int.* **81**, 300–306 (2012).
43. J. Coresh, B. C. Astor, T. Greene, G. Eknoyan, A. S. Levey, Prevalence of chronic kidney disease and decreased kidney function in the adult US population: Third National Health and Nutrition Examination Survey. *Am. J. Kidney Dis.* **41**, 1–12 (2003).
44. J. Kildsgaard, T. J. Hollmann, K. W. Matthews, K. Bian, F. Murad, R. A. Wetsel, Cutting edge: Targeted disruption of the C3a receptor gene demonstrates a novel protective

anti-inflammatory role for C3a in endotoxin-shock. *J. Immunol.* **165**, 5406–5409 (2000).
45. P. Deo, J. B. Keogh, N. J. Price, P. M. Clifton, Effects of weight loss on advanced glycation end products in subjects with and without diabetes: A preliminary report. *Int. J. Environ. Res. Public Health* **14**, 1553 (2017).
46. J. Zeng, M. J. Davies, Evidence for the formation of adducts and S-(carboxymethyl) cysteine on reaction of alpha-dicarbonyl compounds with thiol groups on amino acids, peptides, and proteins. *Chem. Res. Toxicol.* **18**, 1232–1241 (2005).
47. A. M. Watson, J. Li, C. Schumacher, M. de Gasparo, B. Feng, M. C. Thomas, T. J. Allen, M. E. Cooper, K. A. Jandeleit-Dahm, The endothelin receptor antagonist avosentan ameliorates nephropathy and atherosclerosis in diabetic apolipoprotein E knockout mice. *Diabetologia* **53**, 192–203 (2010).
48. M. J. Albert, S. Haridas, D. Steer, G. S. Dhaunsi, A. I. Smith, B. Adler, Identification of a Campylobacter jejuni protein that cross-reacts with cholera toxin. *Infect. Immun.* **75**, 3070–3073 (2007).
49. M. T. Coughlan, G. C. Higgins, T. V. Nguyen, S. A. Penfold, V. Thallas-Bonke, S. M. Tan, G. Ramm, N. J. Van Bergen, D. C. Henstridge, K. C. Sourris, B. E. Harcourt, I. A. Trounce, P. M. Robb, A. Laskowski, S. L. McGee, A. J. Genders, K. Walder, B. G. Drew, P. Gregorevic, H. Qian, M. C. Thomas, G. Jerums, R. J. Macisaac, A. Skene, D. A. Power, E. I. Ekinci, X. W. Wijeyeratne, L. A. Gallo, M. Herman-Edelstein, M. T. Ryan, M. E. Cooper, D. R. Thorburn, J. M. Forbes, Deficiency in apoptosis-inducing factor recapitulates chronic kidney disease via aberrant mitochondrial homeostasis. *Diabetes* **65**, 1085–1098 (2016).
50. P. Shannon, A. Markiel, O. Ozier, N. S. Baliga, J. T. Wang, D. Ramage, N. Amin, B. Schwikowski, T. Ideker, Cytoscape: A software environment for integrated models of biomolecular interaction networks. *Genome Res.* **13**, 2498–2504 (2003).
51. G. Hannon, *FastX-Toolkit* (2009).
52. A. Dobin, C. A. Davis, F. Schlesinger, J. Drenkow, C. Zaleski, S. Jha, P. Batut, M. Chaisson, T. R. Gingeras, STAR: Ultrafast universal RNA-seq aligner. *Bioinformatics* **29**, 15–21 (2013).
53. H. Li, R. Durbin, Fast and accurate short read alignment with Burrows-Wheeler transform. *Bioinformatics* **25**, 1754–1760 (2009).
54. Y. Liao, G. K. Smyth, W. Shi, featureCounts: An efficient general purpose program for assigning sequence reads to genomic features. *Bioinformatics* **30**, 923–930 (2014).
55. M. D. Robinson, D. J. McCarthy, G. K. Smyth, edgeR: A bioconductor package for differential expression analysis of digital gene expression data. *Bioinformatics* **26**, 139–140 (2010).
56. A. Subramanian, H. Kuehn, J. Gould, P. Tamayo, J. P. Mesirov, GSEA-P: A desktop application for Gene Set Enrichment Analysis. *Bioinformatics* **23**, 3251–3253 (2007).
57. A. Fabregat, K. Sidiropoulos, P. Garapati, M. Gillespie, K. Hausmann, R. Haw, B. Jassal, S. Jupe, F. Korninger, S. McKay, L. Matthews, B. May, M. Milacic, K. Rothfels, V. Shamovsky, M. Webber, J. Weiser, M. Williams, G. Wu, L. Stein, H. Hermjakob, P. D'Eustachio, The Reactome pathway Knowledgebase. *Nucleic Acids Res.* **44**, D481–D487 (2016).
58. A. Subramanian, P. Tamayo, V. K. Mootha, S. Mukherjee, B. L. Ebert, M. A. Gillette, A. Paulovich, S. L. Pomeroy, T. R. Golub, E. S. Lander, J. P. Mesirov, Gene set enrichment analysis: A knowledge-based approach for interpreting genome-wide expression profiles. *Proc. Natl. Acad. Sci. U.S.A.* **102**, 15545–15550 (2005).
59. H. Rafehi, A. Balcerczyk, S. Lunke, A. Kaspi, M. Ziemann, H. Kn, J. Okabe, I. Khurana, J. Ooi, A. W. Khan, X. J. Du, L. Chang, I. Haviv, S. T. Keating, T. C. Karagiannis, A. El-Osta, Vascular histone deacetylation by pharmacological HDAC inhibition. *Genome Res.* **24**, 1271–1284 (2014).
60. M. T. Coughlan, F. Y. Yap, D. C. Tong, S. Andrikopoulos, A. Gasser, V. Thallas-Bonke, D. E. Webster, J. Miyazaki, T. W. Kay, R. M. Slattery, D. M. Kaye, B. G. Drew, B. A. Kingwell, S. Fourlanos, P. H. Groop, L. C. Harrison, M. Knip, J. M. Forbes, Advanced glycation end products are direct modulators of β-cell function. *Diabetes* **60**, 2523–2532 (2011).

Acknowledgments: We would like to thank the following people for technical assistance: A. Laskowski, M. Arnstein, A. Morley, F. Y. T. Yap, G. Langmaid, S. Risis, K. Gilbert, E. Grixti, and G. Higgins. We thank P. E. Morgan and H. Ramachandran from the Heart Research Institute for assistance in measuring AGEs by HPLC. We acknowledge the Australian Genome Research Facility (AGRF) for high-throughput sequencing and the support it receives from the Commonwealth. **Funding:** These studies were funded by the National Health and Medical Research Council of Australia (NHMRC) (grant numbers APP586645 and APP1043753) and the Australian and New Zealand Society of Nephrology (ANZSN). **Author contributions:** M.S. was responsible for investigation, methodology and validation, project administration, data curation, data analysis, visualization, and writing the original draft. S.M.T. was responsible for investigation, methodology, project administration, validation, and supervision. R.E.C. was involved in investigation, methodology, analysis, validation, and writing. V.T.-B., T.-V.N., and S.A.P. were involved in investigation and analysis. M.Z. was involved in investigation, validation, data curation, visualization, and data analysis. C.d.P., B.E.H., K.C.S., R.S.L., N.J.K., D.S., A.E.-O., M.J.D., L.D., and P.D. were involved in investigation. M.E.C. and C.R.M. were involved in conceptualization and writing (review and editing). J.M.F. was involved in conceptualization, methodology, supervision, and writing (review and editing). T.M.W. was involved in conceptualization, methodology, and writing (review and editing). M.T.C. conceived and designed the study and was responsible for the methodology, acquired the funding, supervised staff and students, project managed the study, analyzed data, and wrote the paper. **Competing interests:** The authors declare that they have no competing interests. **Data and materials availability:** All data needed to evaluate the conclusions in the paper are present in the paper and/or the Supplementary Materials. Transcriptome sequencing data have been deposited in the Sequence Read Archive, accession number: GSE142261. Microbiota sequencing data have been deposited in the BioProject database, accession number: PRJNA608537.

Submitted 31 August 2020
Accepted 12 February 2021
Published 31 March 2021
10.1126/sciadv.abe4841

Citation: M. Snelson, S. M. Tan, R. E. Clarke, C. de Pasquale, V. Thallas-Bonke, T.-V. Nguyen, S. A. Penfold, B. E. Harcourt, K. C. Sourris, R. S. Lindblom, M. Ziemann, D. Steer, A. El-Osta, M. J. Davies, L. Donnellan, P. Deo, N. J. Kellow, M. E. Cooper, T. M. Woodruff, C. R. Mackay, J. M. Forbes, M. T. Coughlan, Processed foods drive intestinal barrier permeability and microvascular diseases. *Sci. Adv.* **7**, eabe4841 (2021).